TÜBİTAK

Turkish Journal of Earth Sciences

http://journals.tubitak.gov.tr/earth/

Research Article

Turkish J Earth Sci
(2021) 30: 489-515

doi:10.3906/yer-2103-4

Formation age, geochemical characteristics and petrogenesis of syenogranite in Chaihe area, central Daxingan Mountains: Constraints on Late Carboniferous evolution of the Xing'an and Songnen blocks

Dong-Xue LI[1], Chang-Qing ZHENG[1,2,*], Chen-Yue LIANG[1,2], Xiao ZHOU[1]

[1]College of Earth Sciences, Jilin University, Changchun, Jilin, China

[2]Key laboratory of Mineral Resources Evaluation in Northeast Asia, Ministry of Land and Resources, Jilin University, Jilin, China

Received: 11.03.2021 • **Accepted/Published Online:** 20.06.2021 • **Final Version:** 16.07.2021

Abstact: The tectonic evolutionary history between the Xing'an Block (XB) and Songnen Block (SB) in the eastern Central Asia Orogenic Belt (CAOB) has been hotly debated. In this study, we present a series of new data to provide a better constraint on the magmatic process during plate subduction and its implications for the regional tectonic evolution of XB and SB, even the CAOB. The whole-rock geochemistry and zircon U-Pb chronology of syenogranite in the Chaihe area of the Great Xing'an Range have been carried out. The dating results show that the syenogranite was formed in the Late Carboniferous during the 303.1–316.1 Ma. The SiO_2 content of dated samples is around between 65.43%~75.88%, while the total alkali content (K_2O+Na_2O) is 7.23%~10.19%, the content of MgO (0.07%~0.63%) and the value of Mg# is 0.14~0.36. Moreover, they have right-inclined REE distribution patterns [$(La/Yb)_N$ = 1.23–15.61] with slight negative or inappreciable Eu anomalies (δEu = 0.06–0.49). All samples were enriched in LILEs (e.g., Rb and K) and depleted in HFSEs (e.g., Nb, Ta and Ti). Based on these data, combined with their trace element characteristics, we conclude that these rocks in our study area were likely derived from partial melting of the crust. Combining with regional tectonic evolution studies and our petrological and geochemical studies, we propose that they formed in a post-collisional extensional tectonic setting that developed after the amalgamation of the Xing'an and Songnen blocks and closure of the Nenjiang Ocean between them during the Late Carboniferous.

Key words: Carboniferous syenogranite, Great Xing'an Range, Hegenshan–Heihe Suture Zone, central Asia Orogenic Belt

1. Introduction

The Central Asian Orogenic Belt (CAOB) (Jahn et al., 2004) is located between the Siberian Craton and North China Craton. It extends over 5000 km from the Ural Mountains in the west through Kazakhstan, Mongolia, southern Siberia, and eastern China, to the East of the Okhotsk Sea. Northeast China (NE China) is located in the eastern section of the CAOB (Figure 1), which is generally divided into (from west to east) the Erguna block, Xing'an block, Songnen block, Breya-Jiamusi block (Şengör et al., 1993; Xiao et al., 2003; Liu et al., 2010; Xiao et al., 2015; Şengör et al., 2018). In the pre-Mesozoic period, NE China was mainly controlled by the Paleo-Asian Ocean tectonic system, and since the Mesozoic, it has been strongly transformed by the Circum Pacific tectonic domain, which is the key area to solve the tectonic evolution of the eastern section of the CAOB. The Great Xing'an Range is located in the eastern segment of the CAOB between the West Lamulun River-Changchun-Yanji suture zone and the Mongol-Okhotsk suture belt and is divided into the Erguna Block in the northwest and Xing'an massifs in the southeast. The northern Great Xing'an Range contains two major sutures: the Hegenshan–Nenjiang–Heihe suture belt between the Xing'an and Songnen massifs, and the Xinlin–Xiguitu suture zone between the Erguna and Xing'an massifs. The 494–480 Ma post-orogenic granites in the Tahe area (Ge et al., 2005), the 517–504 Ma monzogranites and monzodiorites in the Mohe area (Wu et al., 2005), the 539 Ma K–Ar phlogopite age of the Xinlin ophiolite (Li, 1991), and the recently reported ~647 Ma age of the Jifeng ophiolitic mélange in the central Xinlin–Xiguitu suture zone (Feng et al., 2016) all suggest that the amalgamation of the Erguna and Xing'an massifs occurred at ~500 Ma along the Xinlin–Xiguitu suture zone.

Unlike along the Xinlin–Xiguitu suture belt, accretionary prisms and ophiolites are relatively poorly exposed within the Hegenshan–Nenjiang–Heihe suture belt. This makes the timing of collision between the Songnen and Xing'an Block rather controversial. The Hegenshan ophiolite suggests that the collision occurred

* Correspondence: zhengchangqing@jlu.edu.cn

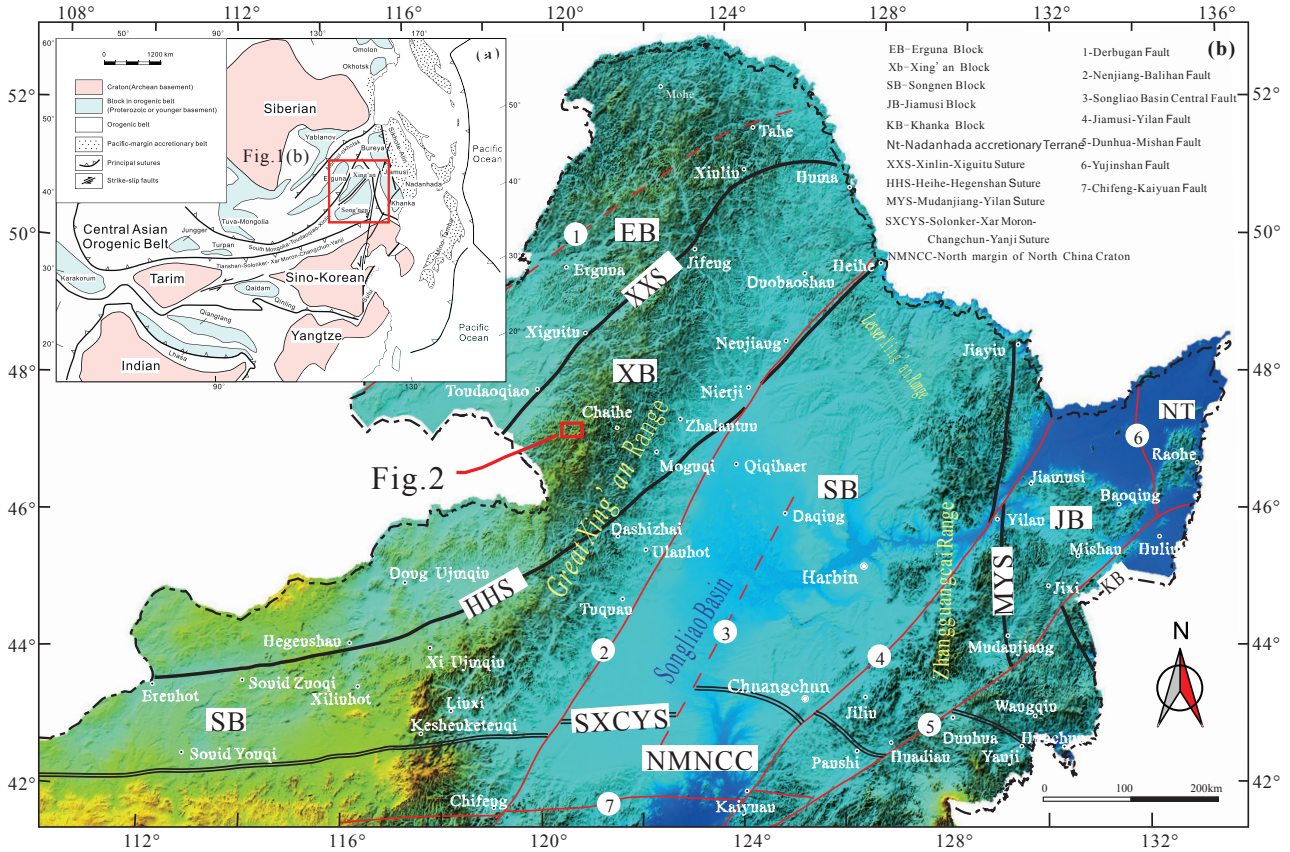

Figure 1. (a) Simplifed tectonic framework of the CAOB and surrounding areas. (b) Tectonic division of the NE China, showing the major blocks, sutures, and main faults (modifed after Liu (2017)).

from the Devonian to the Early Carboniferous between the Erguna-Xing'an and Songnen blocks (Sengör et al., 1993; Sengör and Natal'in, 1996). But some scholars have suggested that the collisional time is from the Silurian to the Cretaceous, the controversy can be summarized as follows: (a) Late Silurian-Devonian (Sengor and Natal'in, 1996; Xu et al.,2013); (b) Devonian (Xu et al.,1997, 2014; Zhao et al., 2014), Late Devonian (Su et al., 1996); (c) Late Devonian-Early Carboniferous (Shao et al., 1991;Hong et al., 1994); (d) Late Early Carboniferous (Zhao et al., 2010a, 2010b; Liu et al, 2012; Li et al., 2014; Zhang et al., 2015); (e) Late Early Carboniferous-Early Late Carboniferous (Liu et al., 2011; Ma et al., 2019); (f) before the Permian (Sun et al., 2000, 2001; Shi et al., 2004; Tong et al., 2010; Li et al., 2016); (g)Triassic (Chen et al., 2000; Miao et al., 2004); (h) Cretaceous (Nozaka and Liu, 2002). Therefore, a series of solutions are needed and the problem goes to an in-depth exploration of all aspects.

Fortunately, recent studies have found that large areas of Late Carboniferous granites, which provide evidence of oceanic plate subduction process, developed in the central area of the central Great Xing'an Range. Therefore, determining the formation ages, petrogenesis, granite origin and continental crust evolution has great significance for the temporal and spatial characteristics of the igneous rock assemblages in the Hegenshan–Heihe suture zone and provide significant tectonic implications. This paper stresses the study on the petrographic, geochemical, and geochronological characteristics of these Late Carboniferous granites, and the tectonic composition and evolutionary history of the suture zone of the Xing'an block and Songnen block are also discussed in the meantime.

2. Geological setting

The NE China, an important tectonic unit in the eastern part of the CAOB (Sengör et al., 1993; Xiao et al. 2015), is composed of several micro-continental blocks including the Erguna Block , Xing'an Block, and Songnen Block (Tang et al., 1990; Wilde et al., 2000; Wilde et al., 2003; Li et al., 2006; Zhou et al., 2010a, 2010b, 2010c; Wu et al., 2011; Zhou et al., 2012; Wang et al., 2013; Xu et al., 2013, 2014; Zheng et al., 2013; Zhou et al., 2015a, 2015b; Ma et al., 2019). The Xing'an block is adjacent to the Ergun block by the Xinlin-Xiguitu suture zone in the north (Feng et al., 2015, 2017; Liu et al., 2017; Feng et al., 2018), and adjacent

to the Songnen block by the Hegenshan–Heihe suture zone (HHS) in the south (Wu et al., 2002; Ma et al., 2019).

The Xing'an Block is mainly composed of the Precambrian basement and Phanerozoic rocks at the top. Its basement mainly consists of metamorphic rocks of the Xinghuadukou Group, which is characterized by a khondalitic sequence that was formed from the Neoarchean to the Paleoproterozoic (Zhou et al., 2013). The Phanerozoic rocks are mainly exposed by volcanic and granitic rocks (HBGMR, 1993; Wu et al., 2000, 2001, 2002, 2003; Ge et al., 2005, 2007; Zhou et al., 2013), and local Paleozoic metamorphic rocks (Miao et al., 2004).

The Songnen Block is located to the southeast of the XB, separated by the HHS (Liu et al., 2010; Han et al., 2011, 2012; Zhou et al., 2011a, 2011b, 2013; Feng et al., 2015). The Songnen Block was known for the Mesozoic Songliao Basin, the Lesser Xing'an Range, and the Zhangguangcai Range. It also has a Precambrian basement composed mainly of granite and gneiss (Wang, 1996), and is overlaid by Palaeozoic sediments (Zhou et al., 2013).

The HHS is generally regarded as the suture zone between the XB and SB (Figure 1b, Ge et al., 2007; Han et al., 2011; Liu et al., 2011; Zhou et al., 2011a, 2011b; Han et al., 2012; Zhou et al., 2013; Feng et al., 2015), and it was first studied as a result of the discovery of ophiolites in the Hegenshan region during exploration for chromium resources in 1954 (Bai et al., 1985). Initially, researchers only proposed a "Hegenshan Suture" in the southern Great Xing'an Range area on the basis of the Hegenshan ophiolites (Bai et al., 1985). Later, however, numerous post-orogenic A-type granites with ages between 260 and 290 Ma were reported in the Heihe area (Wu et al., 2002), and these were coupled with coeval A-type granites in central Inner Mongolia, southern Mongolia, and the eastern Junggar region of Xinjiang (Hong et al., 1995). According to Wu (2002) then suggested a narrow zone of A-type granitic magmatism running west to east along the HHS. The existence and significance of the HHS have now been accepted by more and more researchers on the basis of the belt of A-type granites, the Hegenshan ophiolites in the southwest, and the Duobaoshan porphyry copper deposit (related to oceanic crust subduction) in the northeast (Hong et al., 1995; Ge et al., 2005; Wu et al., 2005; Sui et al., 2006; Ge et al., 2007; Hao et al., 2015).

The study area is located in the central Great Xing'an Range to the northwest of the HHS (Figure 1b). The volcanic rocks and sedimentary rocks and intrusive rocks from late Paleozoic to Mesozoic are widely distributed in the study area and make up the Late Devonian Daminshan Formation, late Carboniferous to early Permian Baoligaomiao Formation, Late Jurassic Manketouebo Formation and Manitu Formation, and early Cretaceous Baiyingaolao Formation (Figure 2). The Daminshan Formation consists of volcanic rocks and sedimentary rocks such as siltstone and tuff lava. The Manketouebo Formation contains a series of acid volcanic rocks including fused tuff, rhyolite and low limestone. The Manitu Formation can be divided into two parts: one is neutral volcanic rocks such as andesite, and the other is acid volcanic rocks such as rhyolite. The Baiyingaolao Formation is characterized by coarse andesite and brecciated tuff. The Late Carboniferous granites exposed in this area have been observed and studied in detail, which are mainly felsic in composition, with a small amount of dark mineral.

3. Sample location and descriptions

Granites are widely developed in the study area, among which the Late Carboniferous granites are the most widely distributed. The Late Carboniferous granites in Jinjianggou Forest Farm, Chaihe area ($\xi\gamma C_2$) which are located at the central Great Xing'an Range. As an important component of the Oroqunchun-Boketu-Arshan-Dongwuqi Granite belt in the Great Xing'an Range, it exposes in the north of Jinjiang Forest Farm, and generally is a large batholith spreading near east and west, covers an area of about 400 km^2 (Figure 2). The Late Carboniferous granites are composed of syenogranite and monzogranite.

The biotite syenogranite (B3213-1, GPS:47°11′22″,120°15′ 37″) is located at the central part of the study area. The hand specimen is light fleshy red (Figure 3a), the mineral composition mainly consists of plagioclase (~25%), orthoclase (~40%), quartz (~25%), and minor dark minerals, such as biotite (~8%) and magnetite (Figure 3b).

The syenogranite (B3220-5, GPS:47°11′37″,120°15′42″) exposed in the central part of the study area. The samples show granite structure and consist of orthoclase (~35%), plagioclase (~15%), quartz (~30%), chlorite (~10%), and a number of dark minerals such as magnetite. Among them, the orthoclase is soiled seriously (Figure 3d).

The biotite syenogranite sample (B4258-1, GPS:47°13′54″,120°04′27″) were taken from the northwest of Jinjianggou Forest Farm. The rock is characterized by medium coarse-grained texture, and the minerals are mainly composed of plagioclase (~10%), quartz (~35%), orthoclase (~50%) and biotite (~5%), and the biotites were chloritic(Figure 3f).

4. Analytical methods

4.1. Zircon U–Pb analyses

Five samples from syenogranite rocks exposed in the study area were selected for U-Pb zircon dating to examine their formation ages. Zircons were separated from whole-rock samples by using the combined heavy liquid and magnetic techniques and then undergone handpicking under a binocular microscope at the Langfang Regional Geological

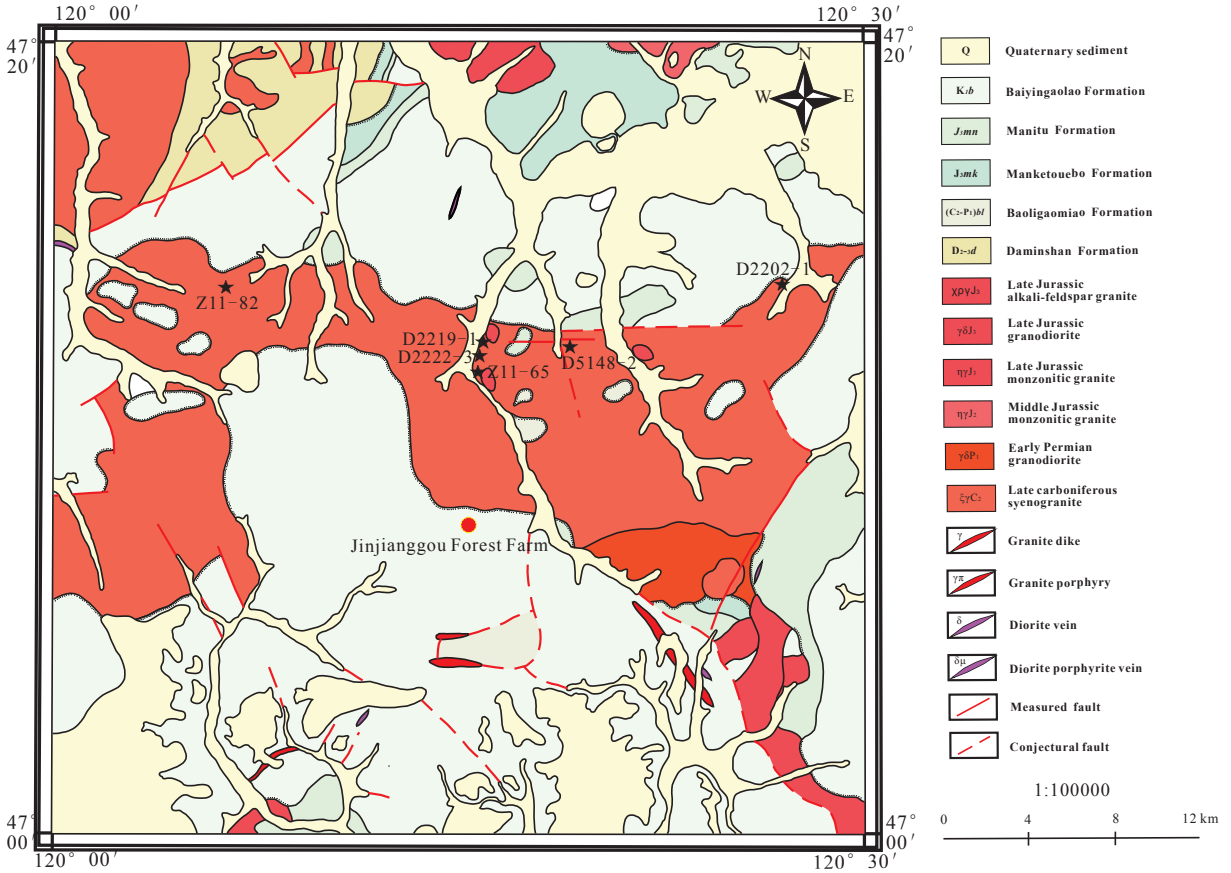

Figure 2. Sketch geological map of the study area with sampling location.

Survey, Hebei Province, China. LA-ICP-MS zircon U-Pb analyses were performed using Agilent 7500A inductively coupled plasma mass spectrometer (ICP-MS) equipped with Coherent COM-PExPro ArF excimer laser, housed at Key Laboratory of Mineral Resources Evaluation of Northeast Asia, Ministry of Natural Resources, Jilin University. All measurements were performed using zircon 91500 as an external standard for age calculation. NIST SRM 610 was used as an external standard for measurements of trace element concentrations. The concentrations of U, Th and Pb elements were calibrated using ^{29}Si as an internal calibrant. ^{207}Pb/^{206}Pb, ^{206}Pb/^{238}U and ^{207}Pb/^{235}U ratios and apparent ages were calculated using ICPMSDataCal (Liu et al., 2008). The age calculations and concordia plots were made using Isoplot (Ver. 3.0) (Ludwing et al., 2003). Zircon U–Pb age data are presented in Table 1.

4.2. Whole-rock major- and trace-element geochemistry

after petrographic examination of major and trace elements, a total of 10 rock samples were carefully selected and powdered in an agate mill. Major element compositions of bulk rock samples were determined by XRF on fused glass disks in the test center of The First Geological Institute of the China Metallurgical Geology Bureau, with analytical uncertainties generally better than ± 5%. Bulk-rock trace element compositions were determined by ICP-MS (Agilent 7500a) after acid digestion of samples in Teflon bombs and dilution in 2% HNO_3 in the same laboratory. During analysis, data quality was monitored by repeated analyses of five rock reference materials (RGW-2, GSR1, AGV-2, BCR-2 and W-2). The accuracy is generally better than 10% for trace and rare earth elements (REE). The analytical results of major and trace elements of the Carboniferous intrusive rocks are listed in Table 2.

5. Results

5.1. Zircon U-Pb geochronology

The zircons in biotite syenogranite (B2222-3) are idiomorphic columnar and with a length of 50–150 μm. Ratios of the length and width range from 1:1 to 5:1, which present obvious oscillatory zoning (Figure 4). Moreover, the zircons have a characteristic of typical magmatic zircon with Th/U ratios of 0.21–1.61. The isotope age of 21 zircon points falls on the concordia curve and its periphery (Figure 5a,b), and the ^{206}Pb/^{238}U age between 282 ± 6 Ma and 339 ± 7 Ma. The weighted average is 303.1 ± 7.2 Ma (MSWD = 6.2).

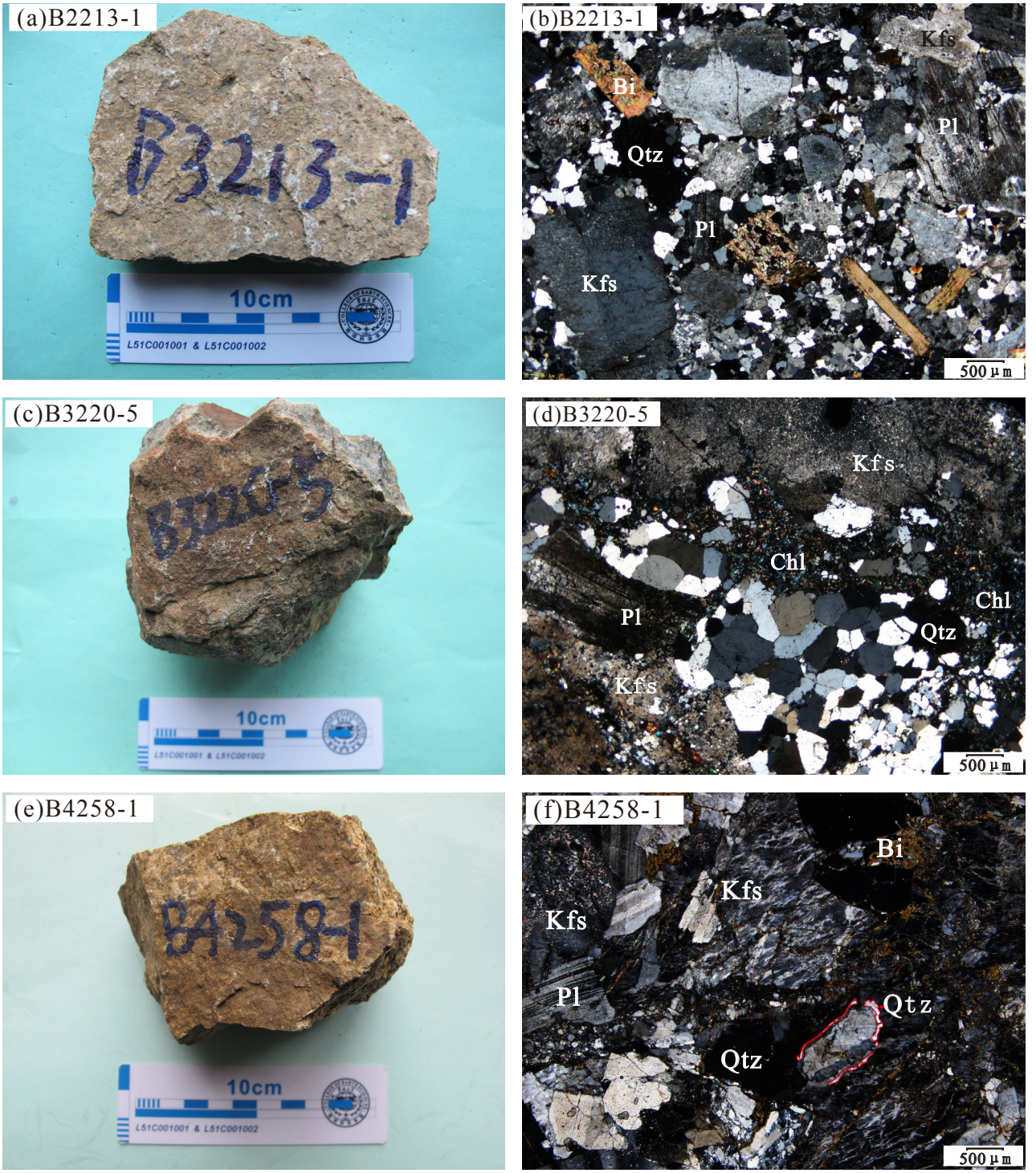

Figure 3. The outcrop photographs and photomicrographs of the Late Carboniferous syenogranites in the central Great Xing'an Range. (a, b) biotite syenogranite. (c, d) syenogranite. (e, f) biotite syenogranite.

The analyzed zircon grains from the syenogranite (B2219-1) are mainly euhedral to subhedral in shape, they have a size range of 50–150 μm with aspect ratios of 1:1–3:1. They are transparent or pale brown to dark, and exhibit oscillatory zoning (Figure 4), and with Th/U ratios from 0.18 to 1.92, indicating a magmatic origin (Hoskin et al.,2003). $^{206}Pb/^{238}U$ ages from 28 analytical spots range from 292 to 331 Ma and yield a weighted mean $^{206}Pb/^{238}U$

Table 1. Zircon LA–ICP–MS U–Pb data for the Late Carboniferous syenogranite in the central Great Xing'an Range.

Sample No.	Th/U	Isotopic ratio								Age/Ma			
		$^{207}Pb/^{206}Pb$	1δ	$^{207}Pb/^{235}U$	1δ	$^{206}Pb/^{238}U$	1δ	$^{208}Pb/^{232}Th$	1δ	$^{207}Pb/^{235}U$	1δ	$^{206}Pb/^{238}U$	1δ
B2219-1													
B2219-1-01	0.3788	0.05308	0.00208	0.36453	0.0143	0.04971	0.00067	0.01567	0.0005	316	11	313	4
B2219-1-02	0.7874	0.05955	0.00452	0.40431	0.02885	0.05023	0.00107	0.01603	0.0006	345	21	316	7
B2219-1-03	1.9231	0.05396	0.00214	0.36334	0.01386	0.04921	0.00069	0.01568	0.00032	315	10	310	4
B2219-1-04	1.0417	0.05878	0.00371	0.40287	0.02289	0.05097	0.00091	0.01766	0.00054	344	17	321	6
B2219-1-05	0.6803	0.0535	0.00227	0.35814	0.01508	0.04893	0.00087	0.01588	0.00049	311	11	308	5
B2219-1-06	0.9524	0.05634	0.00348	0.37572	0.02022	0.049	0.00101	0.01521	0.00047	324	15	308	6
B2219-1-07	1.1628	0.05456	0.00211	0.37096	0.0145	0.049	0.00063	0.01576	0.00029	320	11	308	4
B2219-1-08	1.0309	0.05284	0.00261	0.36478	0.01826	0.04984	0.00073	0.01679	0.00046	316	14	314	4
B2219-1-09	0.8	0.05552	0.00263	0.40579	0.01945	0.05264	0.00088	0.01816	0.00058	346	14	331	5
B2219-1-10	0.7576	0.05496	0.0036	0.39314	0.02682	0.05152	0.00098	0.01599	0.00061	337	20	324	6
B2219-1-11	0.2577	0.05099	0.00203	0.35483	0.01277	0.05065	0.00076	0.01446	0.00042	308	10	319	5
B2219-1-12	0.9259	0.05477	0.00228	0.3815	0.01565	0.05036	0.00068	0.01571	0.0004	328	12	317	4
B2219-1-13	0.4717	0.05771	0.00428	0.39979	0.02362	0.05115	0.00092	0.01655	0.00066	341	17	322	6
B2219-1-14	0.1828	0.05405	0.00247	0.38079	0.01733	0.05085	0.00067	0.01916	0.00089	328	13	320	4
B2219-1-15	1.0989	0.05173	0.00273	0.34714	0.01772	0.04948	0.00096	0.01576	0.00045	303	13	311	6
B2219-1-16	0.9091	0.05592	0.00353	0.37366	0.02347	0.04825	0.0009	0.0158	0.00045	322	17	304	6
B2219-1-17	0.813	0.05294	0.00294	0.35375	0.01929	0.04849	0.00089	0.01611	0.00059	308	14	305	5
B2219-1-18	0.625	0.05258	0.00179	0.35209	0.0111	0.04842	0.0007	0.01471	0.00036	306	8	305	4
B2219-1-19	0.3311	0.05367	0.00205	0.36675	0.01372	0.04945	0.00065	0.01573	0.00046	317	10	311	4
B2219-1-20	0.7937	0.05621	0.00543	0.35648	0.03491	0.04731	0.00124	0.01592	0.00078	310	26	298	8
B2219-1-22	1.0204	0.05595	0.00264	0.37794	0.01734	0.04936	0.00076	0.01559	0.00041	326	13	311	5
B2219-1-23	0.6061	0.05424	0.00359	0.34822	0.02345	0.04632	0.00076	0.01593	0.00059	303	18	292	5
B2219-1-24	0.9259	0.05243	0.00251	0.33911	0.0152	0.0472	0.00062	0.01523	0.00043	297	12	297	4
B2219-1-26	0.5376	0.05166	0.00183	0.3544	0.01256	0.04983	0.00081	0.01569	0.00047	308	9	313	5
B2219-1-27	0.7692	0.05504	0.00329	0.36888	0.01927	0.04995	0.0009	0.01555	0.00054	319	14	314	6
B2219-1-28	0.5076	0.05484	0.00351	0.36456	0.02232	0.04866	0.00103	0.01581	0.0008	316	17	306	6
B2219-1-29	0.5747	0.05289	0.00228	0.36202	0.01498	0.05012	0.00064	0.01538	0.00045	314	11	315	4
B2219-1-30	0.7937	0.05252	0.00318	0.35484	0.02132	0.04987	0.0009	0.01577	0.00054	308	16	314	5

Table 1. (Continued).

B2222-3													
B2222-3-01	0.9346	0.0513	0.00339	0.3414	0.01978	0.04918	0.00095	0.01471	0.00054	298	15	310	6
B2222-3-02	0.6369	0.06847	0.01153	0.43871	0.07246	0.04647	0.00153	0.01414	0.00035	369	51	293	9
B2222-3-04	1.6129	0.05404	0.00403	0.35372	0.02641	0.04708	0.00108	0.01422	0.00041	308	20	297	7
B2222-3-05	0.7463	0.05374	0.0025	0.34652	0.01577	0.04661	0.00077	0.01413	0.00049	302	12	294	5
B2222-3-08	0.9804	0.05559	0.00434	0.37547	0.02808	0.04946	0.00121	0.01619	0.00065	324	21	311	7
B2222-3-09	1.0417	0.05428	0.0149	0.32726	0.08923	0.04373	0.00135	0.01367	0.00085	287	68	276	8
B2222-3-11	0.2882	0.05497	0.00332	0.34157	0.01987	0.04507	0.00073	0.01406	0.00018	298	15	284	5
B2222-3-13	1.1111	0.05736	0.00557	0.35723	0.03512	0.04469	0.00101	0.01337	0.00074	310	26	282	6
B2222-3-15	0.5102	0.05248	0.00382	0.3314	0.0234	0.04645	0.001	0.01329	0.00057	291	18	293	6
B2222-3-16	1.0204	0.05294	0.00422	0.35034	0.02594	0.04764	0.001	0.01339	0.00064	305	20	300	6
B2222-3-17	0.7634	0.05707	0.00937	0.34653	0.04965	0.04769	0.00194	0.01518	0.00117	302	37	300	12
B2222-3-18	0.641	0.05289	0.0025	0.34962	0.01603	0.04707	0.0008	0.01393	0.00074	304	12	297	5
B2222-3-20	1.0417	0.05566	0.00295	0.41687	0.02154	0.05321	0.00095	0.01479	0.00085	354	15	334	6
B2222-3-21	0.2146	0.05556	0.00305	0.36902	0.01962	0.0477	0.00098	0.01541	0.0011	319	15	300	6
B2222-3-22	0.7143	0.05709	0.00537	0.386	0.03601	0.04818	0.00125	0.01484	0.00094	331	26	303	8
B2222-3-23	0.9091	0.05621	0.00564	0.37898	0.03682	0.04934	0.00154	0.014	0.00097	326	27	310	9
B2222-3-25	0.8065	0.0497	0.00287	0.33801	0.01867	0.04923	0.00079	0.01504	0.00063	296	14	310	5
B2222-3-26	0.6849	0.05662	0.00356	0.41974	0.02469	0.05392	0.00109	0.01688	0.00072	356	18	339	7
B2222-3-27	1.1765	0.05136	0.00371	0.33484	0.0217	0.04766	0.00124	0.0146	0.0007	293	17	300	8
B2222-3-28	0.6579	0.05715	0.00293	0.40742	0.02052	0.05149	0.00094	0.01724	0.00067	347	15	324	6
B2222-3-30	0.4255	0.05604	0.00493	0.35415	0.03142	0.04604	0.00127	0.01435	0.00088	308	24	290	8
Z11-65													
Z11-65-02	2.27273	0.05303	0.00413	0.35125	0.02619	0.04879	0.00107	0.01578	0.00035	306	20	307	7
Z11-65-03	0.5988	0.0527	0.00303	0.34592	0.01919	0.04788	0.00065	0.01493	0.00053	302	14	302	4
Z11-65-04	1.13636	0.05527	0.00352	0.3697	0.0203	0.04922	0.00091	0.01497	0.00037	319	15	310	6
Z11-65-05	0.76923	0.05448	0.00486	0.35737	0.03158	0.0484	0.00123	0.01661	0.00105	310	24	305	8
Z11-65-06	0.8	0.05449	0.00483	0.35357	0.02984	0.04834	0.00131	0.01463	0.00075	307	22	304	8
Z11-65-07	0.84746	0.05471	0.0035	0.36601	0.02263	0.0496	0.00083	0.01575	0.00056	317	17	312	5
Z11-65-08	0.67568	0.0524	0.00225	0.34582	0.01386	0.04851	0.00056	0.0152	0.00037	302	10	305	3
Z11-65-09	0.96154	0.05397	0.00253	0.36414	0.01765	0.04885	0.00065	0.01497	0.00037	315	13	307	4
Z11-65-10	0.57471	0.0534	0.00236	0.35751	0.01307	0.04945	0.00072	0.0158	0.00043	310	10	311	4

Table 1. (Continued).

Z11-65-11	0.25189	0.05785	0.00221	0.39666	0.01405	0.04979	0.00055	0.01876	0.00069	339	10	313	3
Z11-65-12	0.54645	0.05269	0.0018	0.35275	0.01232	0.04865	0.00055	0.01481	0.00037	307	9	306	3
Z11-65-13	0.65789	0.05157	0.00158	0.3517	0.01182	0.04939	0.00067	0.01445	0.00033	306	9	311	4
Z11-65-14	0.64935	0.05231	0.0014	0.35531	0.00902	0.04943	0.00049	0.01488	0.00032	309	7	311	3
Z11-65-15	0.3367	0.05177	0.00197	0.35123	0.01309	0.04938	0.00074	0.01493	0.00046	306	10	311	5
Z11-65-16	1.02041	0.0526	0.00234	0.35301	0.01502	0.04926	0.00064	0.01545	0.00032	307	11	310	4
Z11-65-17	0.29499	0.05337	0.00259	0.3626	0.01652	0.04967	0.0007	0.01545	0.00048	314	12	312	4
Z11-65-18	0.77519	0.05199	0.00247	0.34729	0.01622	0.04877	0.00068	0.01602	0.00044	303	12	307	4
Z11-65-19	0.51813	0.05144	0.00136	0.35211	0.00916	0.04964	0.00048	0.01458	0.0003	306	7	312	3
Z11-65-20	0.04606	0.05295	0.00158	0.3605	0.01051	0.04923	0.00052	0.01587	0.00084	313	8	310	3
Z11-65-21	0.68493	0.05274	0.00225	0.35456	0.01415	0.04912	0.00068	0.01494	0.00039	308	11	309	4
Z11-65-22	0.30395	0.05122	0.00143	0.3487	0.00908	0.04952	0.00055	0.01587	0.00038	304	7	312	3
Z11-65-24	0.38462	0.05282	0.00275	0.35461	0.02019	0.04856	0.00073	0.01685	0.00063	308	15	306	4
Z11-65-25	1.21951	0.05492	0.0025	0.36774	0.01693	0.04864	0.00063	0.01492	0.00035	318	13	306	4
Z11-65-26	0.95238	0.0554	0.00292	0.3772	0.0181	0.04986	0.00087	0.01573	0.00038	325	13	314	5
Z11-65-27	0.32362	0.05112	0.00117	0.34679	0.00769	0.04906	0.00042	0.01487	0.00033	302	6	309	3
Z11-65-28	0.40486	0.05421	0.0013	0.36709	0.0086	0.04898	0.00046	0.01613	0.00037	317	6	308	3
Z11-65-29	0.67114	0.05296	0.00289	0.36785	0.0208	0.05032	0.00121	0.01451	0.00052	318	15	316	7
Z11-65-30	0.41841	0.05361	0.00209	0.36375	0.01364	0.04951	0.00067	0.01588	0.00045	315	10	312	4
Z11-82													
Z11-82-01	0.3922	0.05539	0.00134	0.3807	0.00916	0.04969	0.00054	0.01559	0.00039	328	7	313	3
Z11-82-02	0.4049	0.05462	0.00126	0.38388	0.0088	0.05073	0.00048	0.01437	0.00033	330	6	319	3
Z11-82-03	0.3802	0.05401	0.00155	0.38214	0.01025	0.05119	0.00064	0.01543	0.00039	329	8	322	4
Z11-82-04	0.6849	0.05427	0.00128	0.46336	0.01067	0.0617	0.00068	0.01923	0.00032	387	7	386	4
Z11-82-05	0.3802	0.0519	0.00092	0.36835	0.00645	0.05122	0.00045	0.01522	0.00025	318	5	322	3
Z11-82-06	0.7246	0.05677	0.0053	0.38665	0.03519	0.0494	0.00103	0.01536	0.00024	332	26	311	6
Z11-82-07	0.5348	0.05534	0.00233	0.37929	0.01524	0.05007	0.00067	0.01601	0.00046	327	11	315	4
Z11-82-08	0.3676	0.05551	0.00389	0.37155	0.02157	0.05007	0.00097	0.01621	0.00089	321	16	315	6
Z11-82-09	0.6536	0.05103	0.00144	0.35324	0.00958	0.05007	0.00046	0.01609	0.00032	307	7	315	3
Z11-82-10	1.2987	0.05616	0.00176	0.38406	0.01174	0.04941	0.00048	0.01612	0.00034	330	9	311	3
Z11-82-11	0.4505	0.05328	0.00164	0.37022	0.01104	0.05024	0.00052	0.01665	0.00039	320	8	316	3
Z11-82-12	1.0526	0.0532	0.00132	0.36796	0.0084	0.05015	0.00047	0.01598	0.0003	318	6	315	3

Table 1. (Continued).

Z11-82-13	0.4386	0.05499	0.00148	0.3856	0.01028	0.05079	0.00057	0.01641	0.00041	331	8	319	4
Z11-82-14	0.463	0.05536	0.0015	0.38207	0.01037	0.04983	0.00048	0.01567	0.00034	329	8	313	3
Z11-82-15	0.3676	0.05431	0.00128	0.37695	0.00799	0.05031	0.00044	0.01692	0.00033	325	6	316	3
Z11-82-16	0.5464	0.0581	0.00097	0.67549	0.01135	0.08395	0.00072	0.02725	0.0007	524	7	520	4
Z11-82-17	0.4386	0.0509	0.001	0.35775	0.00654	0.05078	0.0006	0.01496	0.00025	311	5	319	4
Z11-82-18	0.3322	0.05316	0.00128	0.37047	0.00869	0.05041	0.00045	0.01627	0.00039	320	6	317	3
Z11-82-19	0.303	0.05299	0.00179	0.37502	0.01215	0.05133	0.00047	0.01609	0.00012	323	9	323	3
Z11-82-20	0.339	0.0529	0.00099	0.36924	0.00667	0.05049	0.00047	0.01632	0.0003	319	5	318	3
Z11-82-21	0.3817	0.05212	0.0014	0.36192	0.00992	0.05015	0.00055	0.01571	0.00037	314	7	315	3
Z11-82-22	0.5435	0.05411	0.00167	0.37371	0.01074	0.05028	0.00056	0.01659	0.00036	322	8	316	3
Z11-82-23	1.1765	0.05115	0.00176	0.34917	0.01107	0.04946	0.00049	0.01441	0.00027	304	8	311	3
Z11-82-24	0.3311	0.05331	0.00116	0.36948	0.008	0.05015	0.00053	0.01577	0.00032	319	6	315	3
Z11-82-25	0.3067	0.05324	0.00128	0.36384	0.00845	0.04956	0.00047	0.01585	0.00035	315	6	312	3
Z11-82-26	1.2658	0.0537	0.0018	0.37267	0.0123	0.0504	0.00054	0.01585	0.0003	322	9	317	3
Z11-82-27	0.5376	0.05475	0.00152	0.38291	0.01045	0.05084	0.00055	0.01663	0.00036	329	8	320	3
Z11-82-28	0.6061	0.05291	0.00237	0.36866	0.01616	0.05085	0.00062	0.01657	0.00046	319	12	320	4
Z11-82-29	0.4016	0.054	0.00178	0.37128	0.01183	0.04998	0.00055	0.01644	0.00044	321	9	314	3
Z11-82-30	1.0101	0.05492	0.00195	0.37346	0.01344	0.04924	0.00063	0.01571	0.00032	322	10	310	4
D5148-1													
D5148-1-01	0.6046	0.0559	0.0015	0.3704	0.0096	0.0481	0.0004	0.0189	0.0002	320	8	303	3
D5148-1-02	0.9276	0.0542	0.0019	0.3739	0.0136	0.05	0.0006	0.0153	0.0002	323	12	315	4
D5148-1-03	0.7286	0.0521	0.0016	0.3583	0.0117	0.0499	0.0005	0.0151	0.0002	311	10	314	3
D5148-1-04	0.4591	0.0538	0.0007	0.3717	0.0052	0.0502	0.0005	0.0147	0.0001	321	5	315	3
D5148-1-05	1.4861	0.0575	0.0029	0.3795	0.0194	0.0479	0.0006	0.0153	0.0004	327	17	302	4
D5148-1-06	0.661	0.0554	0.0017	0.3841	0.0123	0.0503	0.0007	0.0154	0.0005	330	11	316	4
D5148-1-07	0.5858	0.0673	0.0011	0.4692	0.0078	0.0505	0.0004	0.0162	0.0002	391	6	318	3
D5148-1-08	0.8009	0.0632	0.0011	0.4339	0.0083	0.0498	0.0005	0.0167	0.0003	366	7	313	3
D5148-1-09	0.5572	0.056	0.0003	0.3868	0.0022	0.0501	0.0004	0.015	0.0001	332	2	315	3
D5148-1-10	0.7557	0.0527	0.0008	0.3677	0.0057	0.0506	0.0005	0.015	0.0002	318	5	318	3
D5148-1-11	0.7572	0.0537	0.0014	0.3719	0.01	0.0502	0.0005	0.0141	0.0002	321	9	316	3
D5148-1-12	0.6099	0.0526	0.0028	0.3608	0.0195	0.0498	0.0005	0.0143	0.0003	313	17	313	3
D5148-1-13	0.554	0.055	0.0021	0.3872	0.0155	0.0511	0.0007	0.0139	0.0003	332	13	321	4

Table 1. (Continued).

D5148-1-14	0.7562	0.054	0.0025	0.3695	0.0161	0.0497	0.0005	0.0146	0.0003	319	14	312	3
D5148-1-15	0.7149	0.057	0.0023	0.3956	0.0182	0.0503	0.0007	0.0233	0.0008	338	16	316	4
D5148-1-16	0.7441	0.055	0.0015	0.3844	0.0107	0.0507	0.0004	0.0177	0.0003	330	9	319	3
D5148-1-17	0.9152	0.0548	0.0054	0.3697	0.0358	0.0489	0.0006	0.0137	0.0005	319	31	308	4
D5148-1-18	0.9545	0.0544	0.0019	0.3594	0.0141	0.0479	0.0006	0.0179	0.0003	312	12	302	3
D5148-1-19	1.4258	0.0547	0.0021	0.3631	0.0137	0.0482	0.0005	0.0134	0.0005	315	12	303	3
D5148-1-20	0.5676	0.057	0.0015	0.3808	0.0104	0.0485	0.0005	0.0138	0.0002	328	9	305	3
D5148-1-21	0.668	0.0573	0.0026	0.3811	0.0174	0.0483	0.0006	0.0141	0.0002	328	15	304	4
D5148-1-22	0.7159	0.053	0.0025	0.3664	0.0175	0.0502	0.0006	0.0148	0.0003	317	15	315	3
D5148-1-23	0.7316	0.0494	0.004	0.3354	0.0277	0.0492	0.0006	0.015	0.0004	294	24	310	4
D5148-1-24	0.6688	0.0549	0.0031	0.3673	0.0193	0.0486	0.0006	0.0206	0.0009	318	17	306	4
D5148-1-25	0.5311	0.0534	0.0036	0.3605	0.0259	0.0489	0.0006	0.0134	0.0004	313	22	308	4

Table 2. Representative major (wt.%) and trace (ppm) element analyses of the syenogranites

Sample	B2219-1	B2220-1	B3220-5	B3220-10	B4218-2	B4254-1	Z11-82	D5148
SiO_2	67.52	67.04	67.78	67.39	68.46	74.71	75.88	75.34
TiO_2	0.53	0.53	0.48	0.40	0.43	0.15	0.13	0.10
Al_2O_3	15.26	15.61	15.37	15.45	15.05	12.76	12.34	12.89
FeO	2.60	3.15	3.21	1.62	2.28	0.78	0.17	1.08
Fe_2O_3	3.78	4.29	4.96	4.00	3.61	2.06	1.60	0.58
TFeO	6.00	7.01	7.66	5.21	5.53	2.63	1.61	1.60
$^{T}Fe_2O_3$	6.66	7.79	8.52	5.79	6.15	2.92	1.79	1.78
MnO	0.08	0.12	0.24	0.12	0.08	0.06	0.02	0.02
MgO	0.49	0.47	0.51	0.26	0.27	0.19	0.07	0.22
CaO	1.88	1.45	1.37	1.05	1.30	0.25	0.23	0.32
Na_2O	4.15	3.34	3.52	3.82	3.30	3.17	3.55	3.45
K_2O	5.42	5.82	3.88	6.45	6.16	4.62	5.21	5.51
P_2O_5	0.21	0.19	0.20	0.21	0.14	0.06	0.02	0.04
LOS	0.71	0.96	1.75	1.18	1.00	1.30	0.58	0.37
Total	102.61	102.96	103.26	101.93	102.08	100.11	99.81	99.91
A/CNK	0.95	1.08	1.23	1.02	1.04	1.20	1.04	1.05
A/NK	1.20	1.32	1.54	1.17	1.25	1.25	1.07	1.11
AR	3.53	3.32	2.58	4.29	3.74	3.99	5.61	5.22
La	61.68	73.73	70.93	32.56	49.33	34.08	37.47	17.27
Ce	156.06	173.24	150.69	78.03	119.18	76.17	124.88	42.28
Pr	17.78	16.07	18.20	9.45	14.62	8.57	10.91	4.72
Nd	63.90	73.06	64.76	34.84	51.92	28.57	37.71	17.06
Sm	12.34	14.05	12.35	8.50	10.67	5.69	7.93	4.69
Eu	1.58	1.47	1.40	1.35	1.25	0.49	0.15	0.22
Gd	11.46	12.62	11.74	7.95	10.06	5.21	7.64	5.50
Tb	1.63	1.67	1.63	1.27	1.45	0.85	1.22	1.63
Dy	8.17	8.10	8.42	7.32	7.55	5.12	6.86	12.03
Ho	1.47	1.43	1.50	1.37	1.36	1.00	1.26	2.64
Er	4.04	3.78	4.29	3.77	3.84	3.02	3.83	7.63
Tm	0.55	0.53	0.59	0.53	0.57	0.48	0.55	1.49
Yb	3.31	3.10	3.96	3.29	3.60	3.14	3.73	9.20
Lu	0.48	0.47	0.57	0.46	0.55	0.45	0.56	1.07
Y	37.35	35.79	39.57	35.57	35.54	27.01	33.45	74.13
REE	344.45	383.32	351.04	190.71	275.94	172.84	244.70	127.43
LREE	313.34	351.61	318.33	164.74	246.97	153.57	219.05	86.24
HREE	31.10	31.70	32.71	25.97	28.97	19.26	25.65	41.19
LREE/ HREE	10.07	11.09	9.73	6.34	8.53	7.97	8.54	2.09
δEu	0.40	0.33	0.35	0.49	0.36	0.27	0.06	0.13
δCe	1.12	1.16	0.99	1.06	1.06	1.05	1.47	1.11
$(La/Yb)_N$	12.23	15.61	11.74	6.50	8.99	7.12	6.58	1.23
$(La/Sm)_N$	2.97	3.12	3.41	2.27	2.74	3.56	2.81	2.19

Table 2. (Continued).

$(Gd/Yb)_N$	2.80	3.29	2.39	1.95	2.26	1.34	1.65	0.48
Rb	103.30	156.40	283.90	199.60	140.80	192.10	203.30	261.40
Ba	706.53	593.30	562.28	694.99	575.86	274.83	58.28	110.00
Th	23.00	29.01	20.95	10.55	16.57	19.32	15.70	13.14
U	1.55	1.77	1.66	1.65	2.32	4.47	4.70	3.62
Ta	1.57	1.43	1.59	1.47	1.51	1.44	3.46	1.87
Nb	28.19	29.16	28.86	24.83	32.45	16.74	29.29	17.71
La	61.68	73.73	70.93	32.56	49.33	34.08	37.47	17.27
Ce	156.06	173.24	150.69	78.03	119.18	76.17	124.88	42.28
Sr	169.80	127.00	215.00	179.60	156.80	52.82	18.47	40.30
Nd	63.90	73.06	64.76	34.84	51.92	28.57	37.71	17.06
Zr	508.17	507.14	559.42	568.30	558.99	173.70	200.18	106.50
Hf	12.51	12.20	13.91	13.73	13.62	5.32	6.38	5.30
Sm	12.34	14.05	12.35	8.50	10.67	5.69	7.93	4.69
Gd	11.46	12.62	11.74	7.95	10.06	5.21	7.64	5.50
Tb	1.63	1.67	1.63	1.27	1.45	0.85	1.22	1.63
Y	37.35	35.79	39.57	35.57	35.54	27.01	33.45	74.13
Yb	3.31	3.10	3.96	3.29	3.60	3.14	3.73	9.20
Lu	0.48	0.47	0.57	0.46	0.55	0.45	0.56	1.07
Cs	5.75	13.17	10.26	3.71	7.83	7.13	7.28	
Ga	22.82	22.56	23.45	22.37	23.58	18.66	22.71	
Cu	7.49	25.52	11.98	9.62	21.05	5.62	8.72	20.50
Zn	72.62	515.70	1356.41	76.65	269.35	84.41	113.49	33.90
P	901.96	814.74	854.96	898.96	622.63	242.99	89.00	157.10
Ti	3197.73	3177.07	2849.76	2380.80	2560.37	907.92	799.93	599.35
K	44994.06	48279.48	32234.67	53519.68	51101.17	38377.77	43267.35	36020.24
Al	80760.06	82590.72	81342.21	81765.59	79670.85	67529.38	65306.63	68217.38

age of 311.6 ± 3.1 Ma with MSWD = 2.8 (Figure 5c), which is interpreted as its crystallization age.

The zircons from biotite syenogranite (Z11-65) are commonly euhedral to subhedral. They are oval or prismatic in shape with long axes of 50–150 μm and length-to-width ratios of 1:1–3:1. The zircon grains show wide oscillatory zoning (Figure 4) and with Th/U ratios from 0.05 to 2.27, which is consistent with a magmatic origin. Twenty-eight analyses of U–Pb ages yielded a concordant $^{206}Pb/^{238}U$ age of 309.3 ± 1.4 Ma (MSWD = 0.62) (Figure 5d). This age is interpreted as the crystallization age of the biotite syenogranite.

The analyzed zircon grains from the syenogranite (Z11-82 and D5148-1) have the same characteristic in zircon crystals and shape. They are commonly dark, because of the high Th/U ratios. Meanwhile, they are euhedral, with long axes of 100–200 μm and mainly show fusiform shapes except few prismatic or slightly rounded zircon grains (Figure 4). The clearly tiny oscillatory growth zoning and Th/U ratios (0.05–1.48) indicate their magmatic origin. The Z11-82 ages of twenty-eight zircon grains from a coherent concordant group (Figure 5e) and define a weighted mean $^{206}Pb/^{238}U$ age of 316.1 ± 1.3 Ma with an MSWD of 1.13. $^{206}Pb/^{238}U$ ages from 25 analytical spots of D5148-1 range from 302 to 321 Ma and yield a weighted mean $^{206}Pb/^{238}U$ age of 311.6 ± 2.5 Ma with MSWD = 3.4 (Figure 5f). We, thus, interpret these ages as their crystallization ages.

5.2. Whole-rock major- and trace-element geochemistry

The major and trace element geochemical data for the Late Carboniferous syenogranites in the study area are listed in Table 2.

The Late Carboniferous syenogranites have high SiO_2 contents of 67.04 wt%–75.88 wt%, high $^{T}Fe_2O_3$ (1.78 wt%–7.79 wt%), CaO (0.23 wt%–1.88 wt%), and MgO (0.07 wt%–0.51 wt%) contents, and low Mg# values of 0.14–0.36. Figure 6a indicates that these alkali-feldspar granites

are plotted in the granite area and quartz monzonite area in the TAS petrographic classification diagram. They have high K_2O contents of 3.88 wt%–6.45 wt%, total alkali (K_2O + Na_2O) contents of 7.29 wt%–10.19 wt%, and K_2O/Na_2O ratios of 1.10–1.87 (average = 1.25) characteristic of K-rich granites (Barbarin et al., 1999), major of which plot in the alkaline field in an AR–SiO_2 diagram (Figure 6c). They have Al_2O_3 contents of 12.34 wt%–15.93 wt% with A/CNK ($Al2O_3$/(CaO + Na_2O+K_2O)) ratios of 0.89–1.23 and typical of weakly peraluminous signatures, as shown on the A/NK-A/CNK diagram in Figure 6b, which are suggestive of the characteristics of aluminium A-type granite (Figure 6d).

The total amount of rare earth elements in the Late Carboniferous syenogranites is 127.43~383.32, and it can be seen that the total amount of rare earth elements decreases with the increase of SiO_2 content. The samples are enriched in light rare earth elements (LREEs), depleted in heavy rare earth elements (HREEs) (LREE/HREE = 2.09–11.09), which has right-tilted characteristics in the rare earth element chondritic meteorite standard partition cobweb diagram (Figure7a). The LREE and HREE have different degrees of fractionation ($(La/Yb)_N$ = 1.23~15.61), and the fractionation degree between LREE is relatively strong, while the ratio between HREE is relatively gentle($(La/Sm)_N$ = 2.19~3.56, $(Gd/Yb)_N$ = 0.48~3.29). The δEu range is 0.06–0.49, and obvious negative anomalies can be seen in Figure 7, which may be caused by part of plagioclase residue in the source region during the evolutionary process, or it may be caused by obvious separation and crystallization. According to previous studies, if the distribution pattern of rare earth elements in acid volcanic rocks is similar to seagull, the acid volcanic rocks are similar to A-type granite or highly differentiated I-type granite.

A primitive-mantle-normalized trace element spider diagram shows that these syenogranites are enriched in large ion lithophile elements (LILEs; e.g., Rb and K), depleted in high field strength elements (HFSEs) such as Ta (1.43–3.46 ppm), Ti (599.35–3197.73ppm) (Figure 7b). These geochemical characteristics of the syenogranites are similar to those of the coeval intermediate-acidic intrusive rocks in the northern Great Xing'an Range (Zhou et al., 2005; Sui et al., 2009a, 2009b; Zhao et al., 2010a, 2010b; Qu et al., 2011; Cui et al., 2013).

6. Discussion

6.1. Genetic type and petrogenesis of the Carboniferous magmatism

The aluminum index of the dated samples is 0.95–1.23, although two samples are peraluminous (A/CNK>1.1), which slightly showing the characteristics of S-type granite

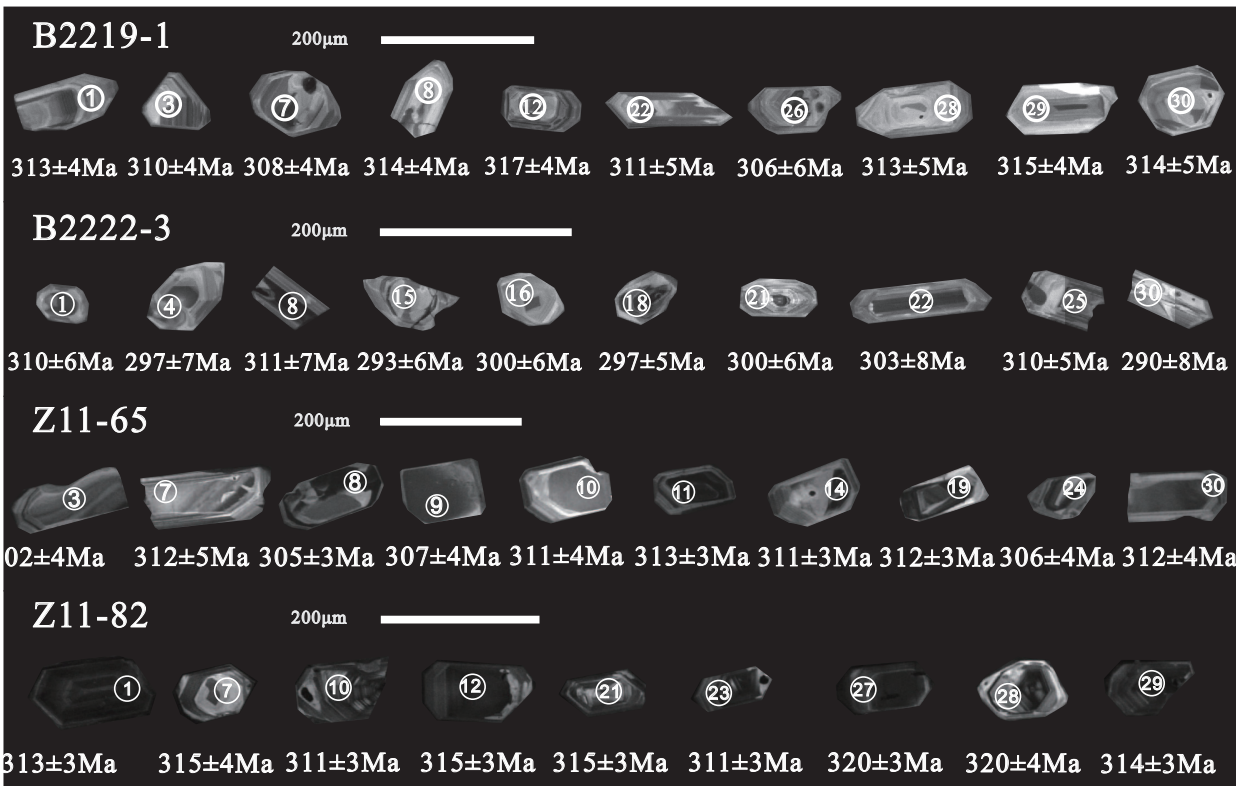

Figure 4. Representative CL images of zircons from the Late Carboniferous in the central Great Xing'an Range.

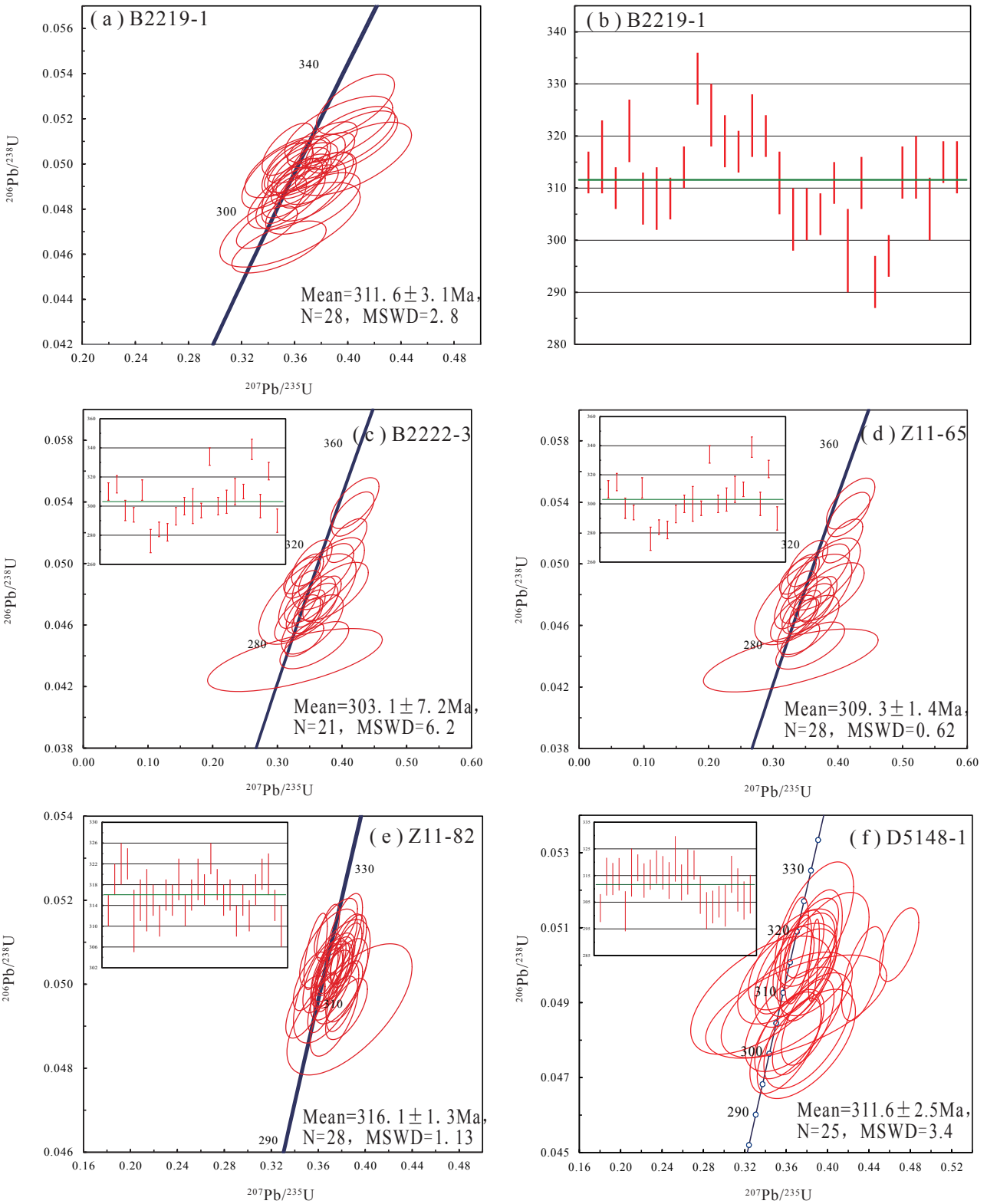

Figure 5. $^{206}Pb/^{238}U$ vs $^{207}Pb/^{235}U$ concordia plots of investigated samples. Errors are 1σ.

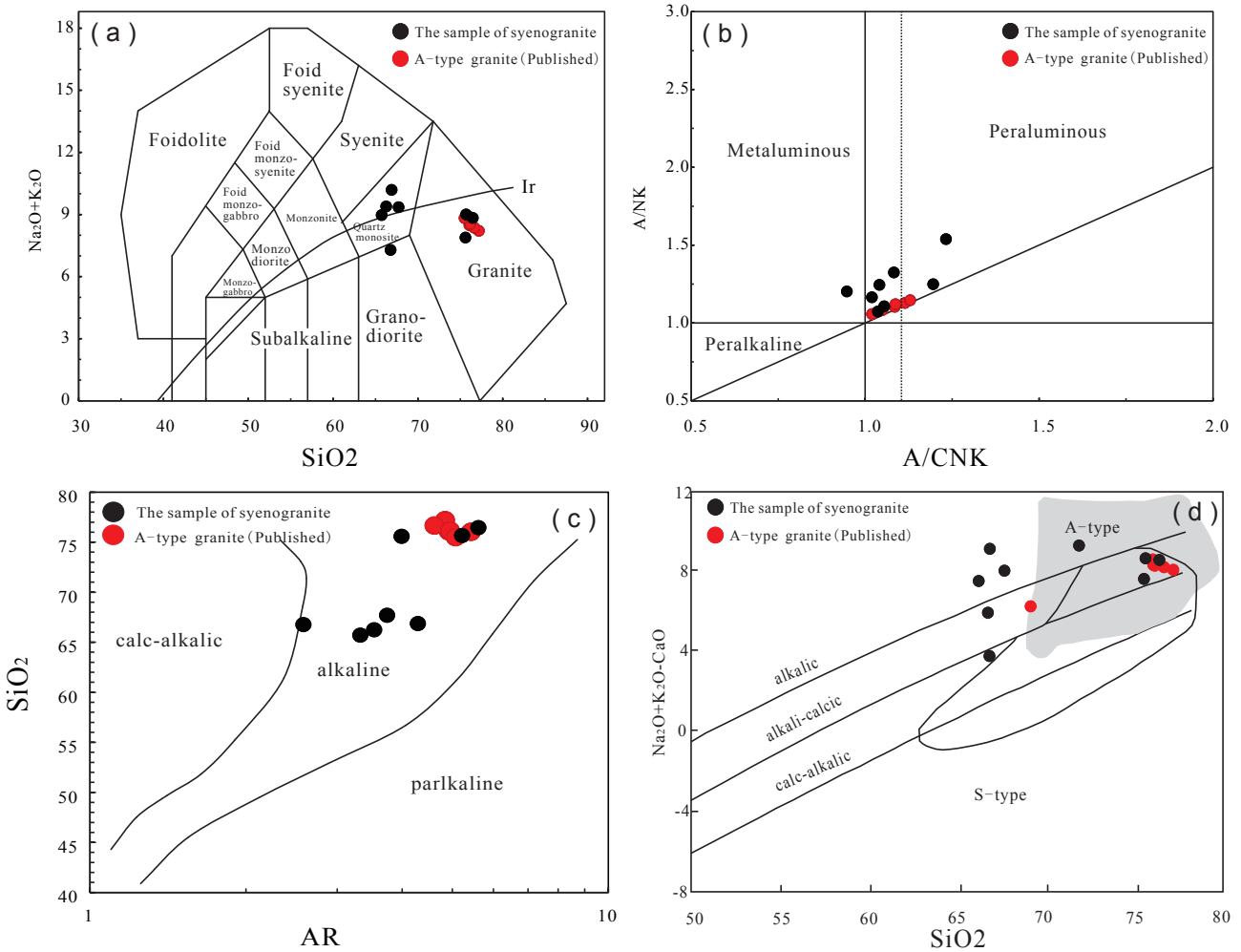

Figure 6. (a) SiO_2 versus (Na_2O+K_2O) (Middlemost et al., 1994; Peccerillo et al., 1976), **(b)** A/CNK versus A/NK, **(c)** AR versus SiO_2, **(d)** SiO_2 versus (Na_2O+K_2O-CaO) (Forst et al.,2001) diagrams for the Carboniferous syenogranite samples in the northern Great Xing'an Range. The boundary lines in **(b)** are from Irvine and Baragar (1971) and Peccerillo and Taylor (1976), respectively (published data from Mao (2019).

overaluminity. But, petrographic identification shows that they do not contain aluminum-rich minerals, and the samples have an obvious negative Eu anomaly, which indicates that the rocks are strongly differentiated during their formation.

Comprehensive analysis shows that the analyzed samples do not belong to S-type granite. Geochemical characteristics of syenogranites share similarities with typical A-type granite (Collins et al., 1982; Whalen et al., 1987; Wu et al., 2002; Li et al., 2010; Zhang et al., 2010; Wu et al., 2011; Zhang et al., 2011; Cui et al., 2013; Li et al., 2013; Zhang et al., 2013a, 2013b; Mao et al., 2019; Qian et al., 2018; Shi et al., 2019; Tian et al.,2018; Ma et al.,2019), which indicate the crustal source of magma. Given the fairly high FeO^T values (1.60%–7.66% with an average of 4.66%) and fairly low Rb contents (103.3×10^{-6}–283.9×10^{-6}) of the syenogranites from the Chaihe area and the fact that all the samples plotted in the A-type granite field in the diagrams of (Na_2O+K_2O)/CaO vs (Zr + Nb + Ce + Y), FeO^T / MgO vs (Zr + Nb + Ce + Y), Zr vs 10000Ga/Al, Nb vs 10000Ga/Al, (K_2O+MgO) vs 10000Ga/Al, K_2O/MgO vs 10000Ga/Al, Ce vs 10000Ga/Al and (Na_2O+K_2O)/CaO vs 10000Ga/Al (Figure 8). CL images of dated zircon show euhedral–subhedral shapes and typical oscillatory and straight rhythmic stripes zoning, suggesting a magmatic origin with high Th/U ratios (0.05–2.27). We believe that the LA-ICP-MS zircon U–Pb ages represent the crystallization ages of the syenogranites.

By the means of contrast, a study is carried through both syenogranites in the Chaihe area and the Late Carboniferous granites in the CAOB (Qian et al.,2018; Shi et al., 2019; Tian et al., 2018; Ma et al., 2019; Mao et al., 2019; Ma et al., 2020). Results can clearly show that their partition curves have a similar trend with A-type granite

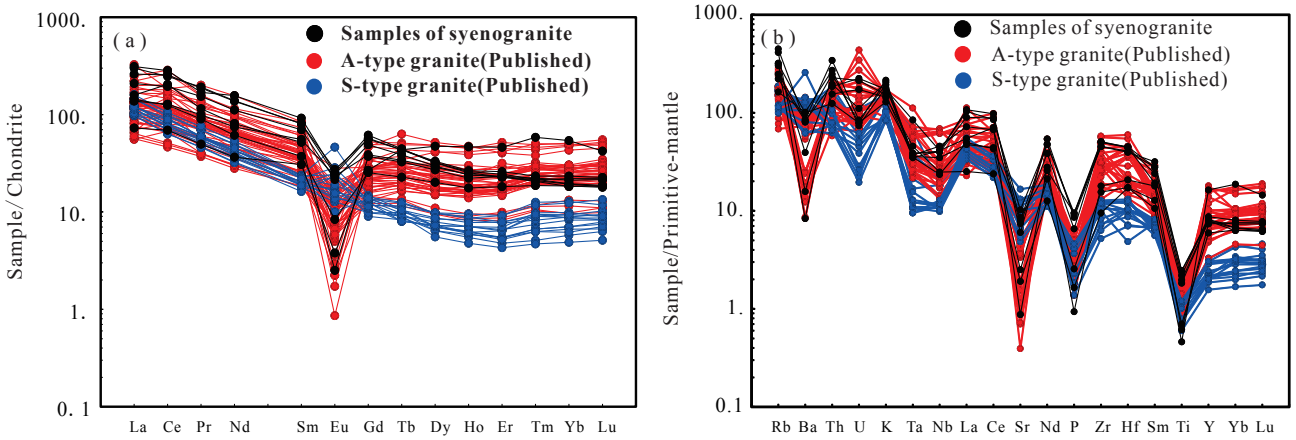

Figure 7. Chondrite-normalized REE patterns (a) and primitive-mantle-normalized trace element spidergrams (b) for the Carboniferous intrusive rocks in the northern and central Great Xing'an Range Chondrite and primitive-mantle values are from Boynton (1984) and Sun and McDonough (1989), respectively (published data from Qian et al.,2018; Ma et al.,2019,2020; Shi et al., 2018; Chen et al., 2019; Tian et al., 2018).

(Figure 7). The La/Sm ratios of analyzed samples are in the range of 3.68–5.99, which are relatively high and change within a certain range. These data indicate that the magma may come from the crustal material or may be influenced by the crustal material during the recrystallization. In addition, it can be known that the Ti/Y of crust-derived magma is less than 100, Ti/Zr is less than 20 (Pearce et al., 1983), and the Ti/Y and Ti/Zr ratios of our analyzed samples are 8.09–88.78 and 4.00–6.29, respectively. In the Yb-Sr diagram (Figure 9a,), the samples fall in the area of Zhe-Min type granite and Nanling type granite, showing the characteristics of low Sr (Zhang et al., 2006). According to the magma source diagram (Figure 10), it can be concluded that the magma of the Late Carboniferous syenogranite in the Chaihe area originated from the crust (Zhang et al., 2008). In the meanwhile, the samples have a positive correlation trend, showing the characteristics of partial melting in the La/Sm-La diagram (Figure 9b). Thus, we propose that the Late Carboniferous syenogranites in the Chaihe area are most consistent with the origin of the partial melting of the crust.

6.2 Nature and distribution of the Carboniferous magmatism

All our analyzed samples were previously mapped as Proterozoic basement based on K–Ar dating and lithostratigraphic relationships (Hu et al., 1995). Zircon U–Pb dating is current considered the best solution for determining the ages of the magmatic rocks in this region. There are some dating results supported by the widespread occurrence of coeval magmatism and mineralization in the northern Great Xing'an Range (Figure 11 and Table 3). For example, the LA-ICP-MS zircon U–Pb ages of many basic intrusive rocks from the Tahe area, Jalaid Banner and Tayuan from 300 Ma to 333 Ma (Zhou et al., 2005; Wu et al., 2011; Wang et al.,2013; Feng et al.,2015; Ma et al.,2020). The SIMS zircon U–Pb dating for metagabbro from the Jiwen and Tayuan area gave ages varying from 306 Ma to 315 Ma (Feng et al., 2015). Similarly, the LA-ICP-MS zircon U–Pb dating for syenogranite or monzonitic granite from Ganhe, Jalaid Banner, Langfeng, Lapou, Longzhen, Mouguqi, Quansheng, Shierzhan, Taerqi, Tayuan, Xing'an, Zhalantun and Zhengdashan area within the Erguna-Xing'an block are 304 ± 5.0 Ma(Wu et al.,2011), 320.6 ± 3.7 Ma (Ma et al.,2020), 337 ± 8 Ma (Wu et al.,2002), 325 ± 3 Ma (Zhang et al., 2013a), 316 ± 4 Ma (Zhang et al.,2010), 321 ± 3.5 Ma (Ma et al., 2019), 294–322 Ma (Cui et al., 2013), 298 ± 2 Ma (Sui et al.,2009b), 313–335 Ma (Zhang et al., 2011), 318–330 Ma (Feng et al., 2015), 309 ± 4 Ma (Wu et al., 2011), 301 ± 3 Ma (Wu et al., 2002), 315 ± 4 Ma (Zhang et al., 2008), respectively. In addition, the syenogranite of Daiheishan and Heihe and Duobaoshan, the granodiorite of Jalaid Banner, Taerqi and Yakeshi, the rhyolite and granite porphyry of Mouguqi yield zircon has the U-Pb ages of 292 ± 4 Ma, 322 ± 5 Ma (Wu et al.,2002) and 299.3 ± 2.8 Ma (Qu et al.,2011), 320 ± 1 Ma (Wu et al.,2011; Zhang et al.,2011) and 331.2 ± 3.7 Ma (Zhao et al., 2010a), 307.5 ± 2.3 Ma, 312.6 ± 2.9 Ma and 309.8 ± 3.6 Ma (Ma et al.,2019), respectively. All these data suggest that all the reported zircon ages recorded the Carboniferous magmatic events in the study area.

6.3 Late Carboniferous evolution of the Xing'an and Songnen blocks

Traditionally, the tectonic setting of A granite is defined as the "non-orogenic" extensional environment. After reviewing previous findings and examining a wealth of A-type granites from typical tectonic backgrounds, Eby (1990,1992) divided these granites into the A_1 and A_2 subtypes. The former represents granites that were intruded

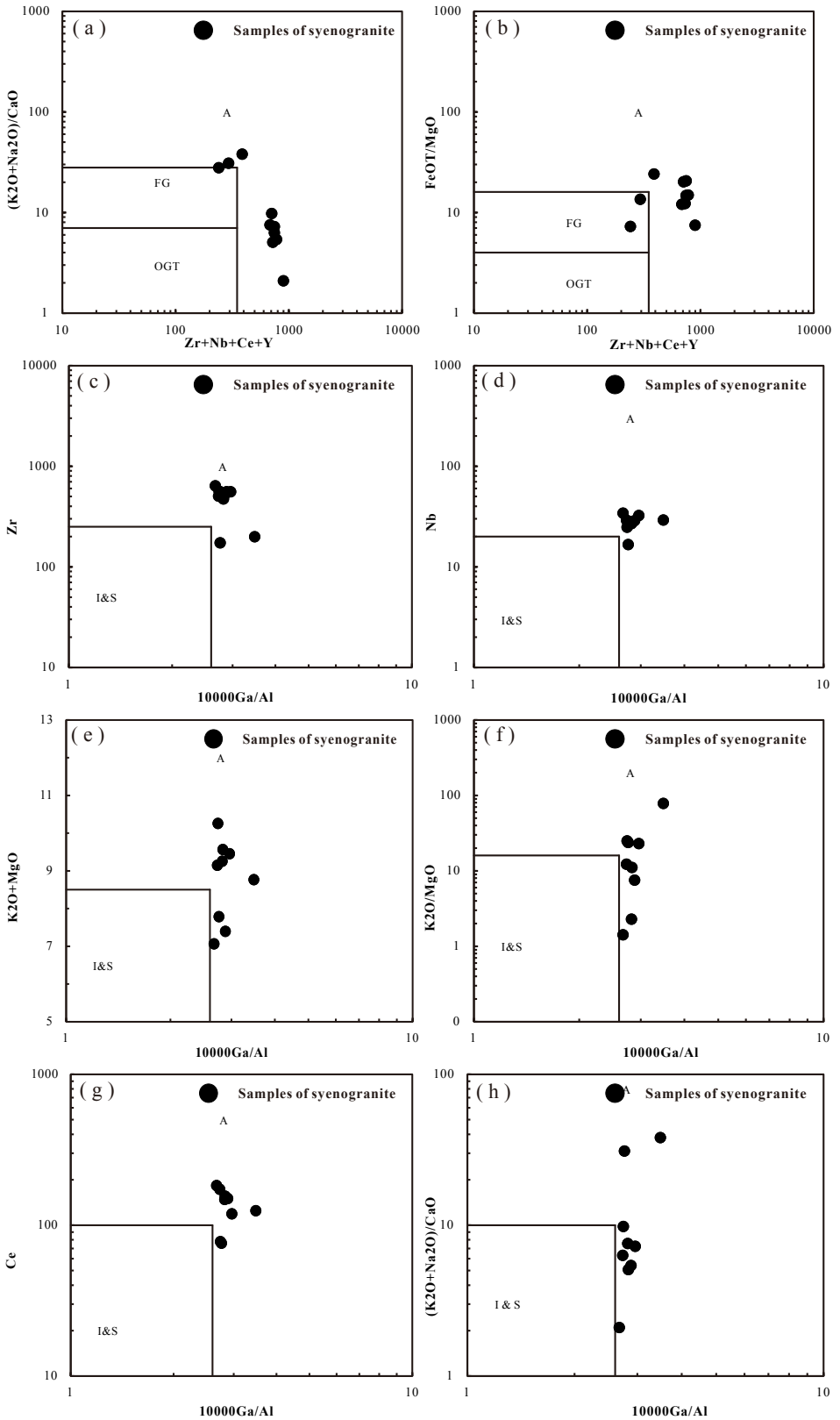

Figure 8. (a) (K2O+Na2O) versus CaO - (Zr+Nb+Ce+Y), (b) FeOT versus MgO - (Zr+Nb+Ce+Y), (c) Zr-10000Ga versus Al diagram, (d) Nb-10000Ga versus Al diagram (e) K2O+MgO-10000Ga versus Al diagram (f) K2O versus MgO-10000Ga versus Al diagram, (g) Ce-10000Ga versus Al diagram (h) (K2O+Na2O) versus-10000Ga versus Al diagram (modified after Whalen et al., 1987).

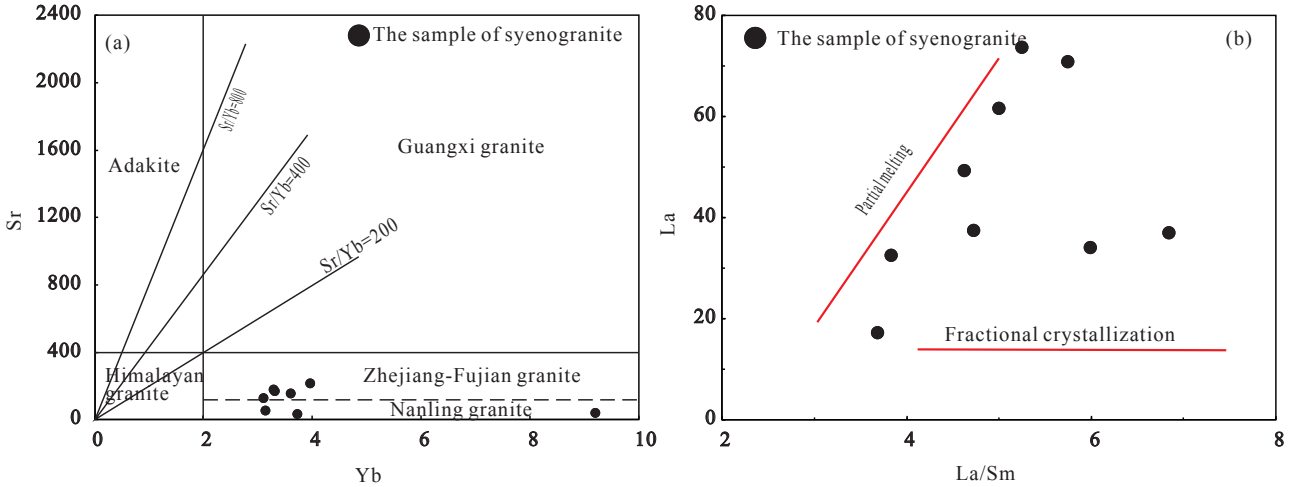

Figure 9. (a) Sr versus Yb diagram of different types of granite (modified after Zhang et al., 2006). **(b)** La versus La/Sm diagram.

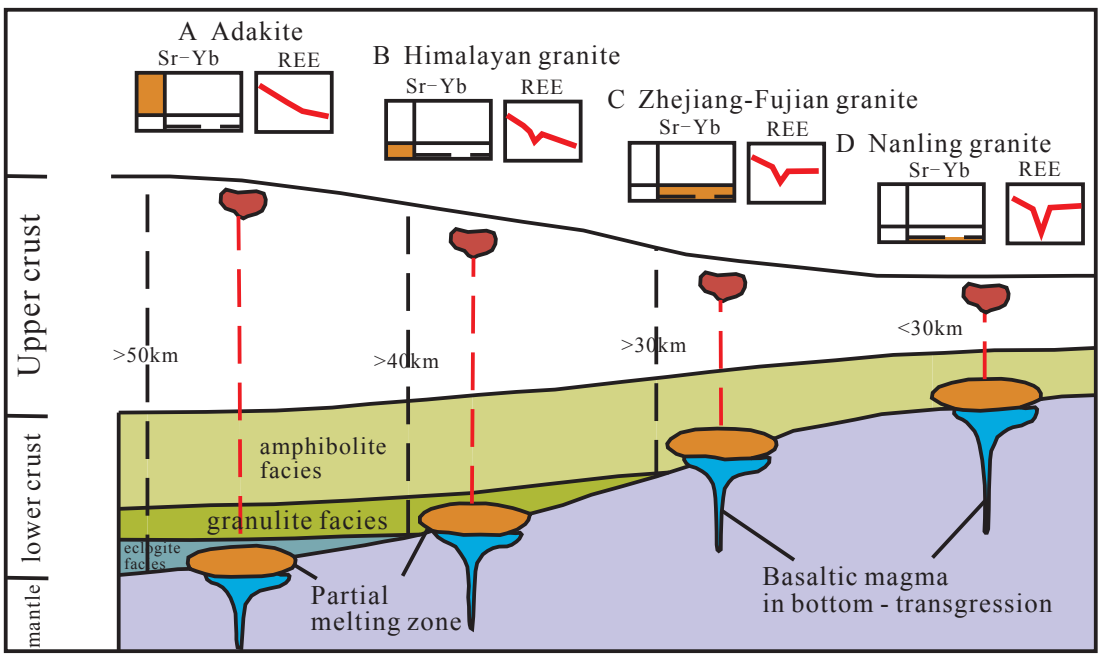

Figure 10. Patterns of different types of granite formation (modified by Zhang et al., 2008).

in a non-orogenic setting during continental rifting or intraplate magmatism (e.g., hotspot or mantle plume activity); the latter involves a broader range of tectonic settings, typically a post-collisional extension background. In the Nb-Y-Ce and Nb-Y-3Ga diagrams (Figure 12), the syenogranites samples from the Chaihe area fall within the A_2-type granite field, which has the same distribution as the published A-type granites in the HHS (Eby et al.,1992). The A_1 field is emplaced in anorogenic settings such as plumes, hotspots, or continental rift zones. The A_2 group is related to a cycle of subduction-zone, or continent-continent collision magmatism in the crust and emplaced in a variety of tectonic settings. Since this type of granite covers a wide range of tectonic background, the geochemical properties of the rocks and the regional geological backgrounds must be considered to determine the exact tectonic backgrounds. The trace elements in the Chaihe A-type syenogranites samples are mainly represented by the enrichment of high field strength elements (HFSES), Th, Rb and K, as well as the large ion lithophile elements (LILES), Ba, Nb, Sr, P and Ti. Obviously, these elements are typical continental magma arcs. Most recent findings have indicated that A_2-type granites can also be formed in volcanic arc settings, such as lithospheric extension in

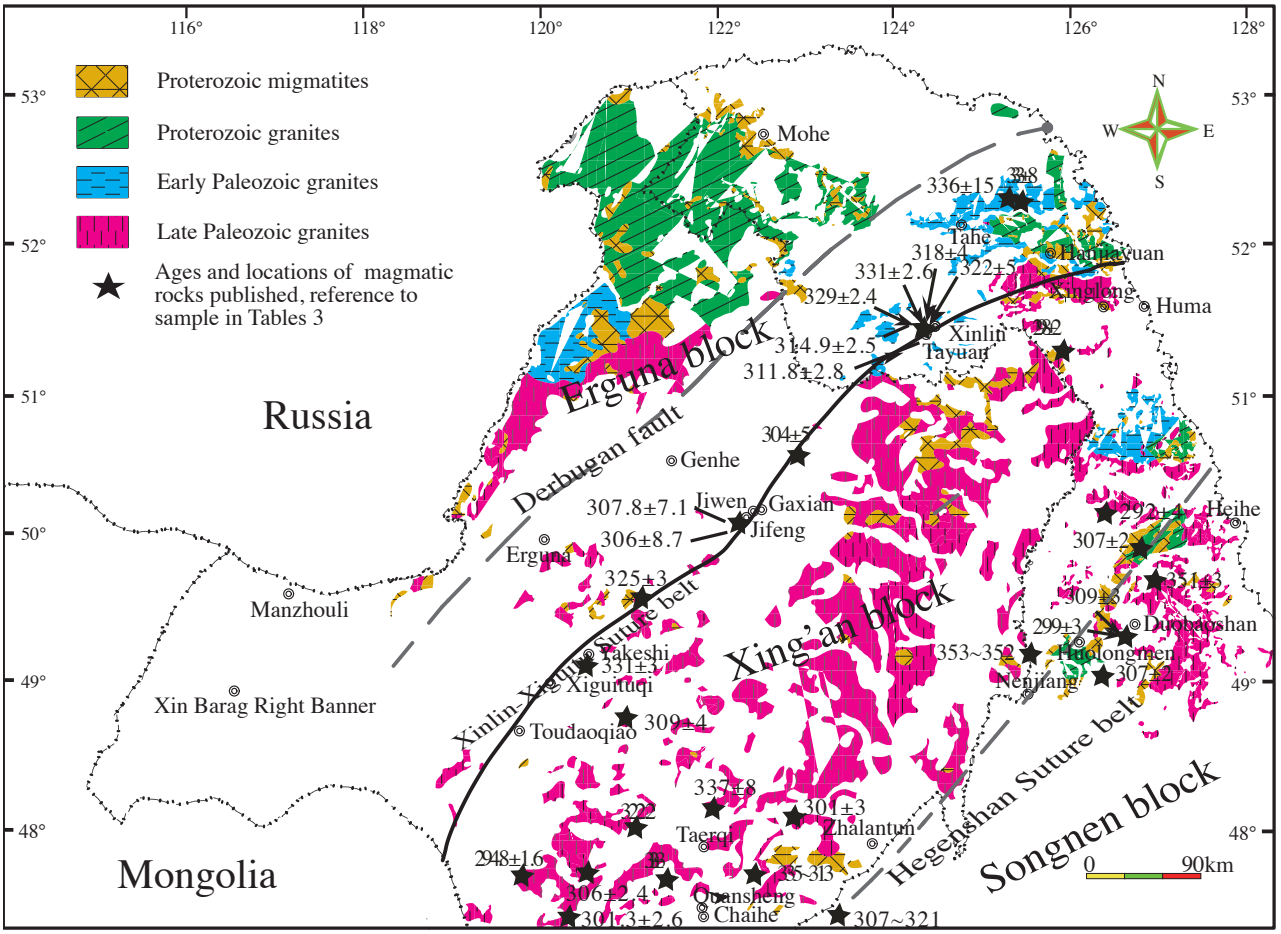

Figure 11. Tectonic division of the Great Xing'an Range and the distribution of the Carboniferous U–Pb zircon ages (modified after Zhang et al., 2013a,b; data listed in Table 3).

response to plate subduction (Guo et al., 2008; Jiang et al., 2008; Zhou et al., 2008). Similarly, the syenogranites mainly plot in the post-collisional field in the tectonic discrimination diagrams (Figure 13a-d), indicating a volcanic arc setting (Pearce et al., 1984). Taking the part of characteristics of A-type granite together with the regional geological setting, we propose that they mainly formed in an extensional tectonic setting.

According to the published age data (Table 3), the HHS A-type granite belt was mostly formed between the Late Carboniferous and Early Permian, and the A-type granites from Chaihe area formed during 303–316 Ma, i.e. the Late Carboniferous. In addition, the Late Carboniferous S-type granites (320 Ma) in the Moguqi area of the central Great Xing'an Range were formed under the background of the thickened crustal syn-collision structure (Ma et al., 2020). The rhyolite (312 Ma) interlayer in the Baoli Gaomiao Formation in the Moguqi area showed the characteristics of typical A-type granites that indicate the tectonic background of the extension zone, which once again confirms our view (Ma et al., 2019). Thus, we propose that the collision and assembly of the XB and SB are postulated to have occurred before the Late Carboniferous.

J. B. Zhou and Wilde (2013) and J. B. Zhou (2015a) indicated that the Hegenshan ophiolite represents the suture between the XB and SB in the Late Palaeozoic. Miao (2008) and Jian (2010) considered that the Hegenshan ophiolite was formed during the Carboniferous, which is supported by the presence of Late Carboniferous–Early Permian conglomerates unconformably overlying the Hegenshan ophiolitic complex in the Wusinihe and Xiaobaliang areas, Hegenshan (Bao et al., 2011; Zhou et al., 2015a). These pieces of evidence constrain the postulation that the Hegenshan ophiolite was emplaced before the Late Carboniferous. According to some scholars based on the 216 Ma metamorphic age of the Xinkailing-Keluo complex in the northwestern part of the Xiao Hinggan Mountains (Miao et al., 2003) and the gabbro age of the Hegenshan ophiolite from 290 to 298 Ma (Miao et al., 2008), they believe that the collision and fusion of the

Table 3. Goechronological ages of Late Carboniferous granitic rocks exposed in the Great Xing'an Range.

Order	GPS location	LIthology	Method	Age (Ma)	References
1	Daheishan (50°14′05″N, 126°28′10″E)	Syenogranite	Zr.TIMS	292.0 ± 4.0 Ma	Wu et al., 2002
2	Duobaoshan(50°00′20″N,125°50′06″E)	Monzonitic granite	Zr.SHRIMP	309.0 ± 3.0 Ma	Qu et al., 2011
3	Duobaoshan(50°00′20″N,125°50′07″E)	Syenogranite	Zr.SHRIMP	299.3 ± 2.8 Ma	Qu et al., 2011
4	Ganhe	Monzonitic granite	Zr.LA-ICP-MS	304.0 ± 5.0 Ma	Wu et al., 2011
5	Heihe	Syenogranite	Zr.TIMS	322 ± 5 Ma	Wu et al., 2002
6	Jalaid Banner (46°48′35″N, 122°45′34″E)	Diabase	Zr.LA-ICP-MS	317.3 ± 1.1 Ma	Wang et al., 2013
7	Jalaid Banner (46°48′35″N, 122°45′35″E)	Gabbro	Zr.LA-ICP-MS	328.0 ± 1.3 Ma	Wang et al., 2013
8	Jalaid Banner (46°48′35″N, 122°45′36″E)	Giorite	Zr.LA-ICP-MS	325.2 ± 0.9 Ma	Wang et al., 2013
9	Jalaid Banner (47°23′55″N, 122°19′32″E)	Gabbro	Zr.LA-ICP-MS	300.6 ± 3.3 Ma	Ma et al., 2020
10	Jalaid Banner (47°23′59″N, 122°19′56″E)	Granodiorite	Zr.LA-ICP-MS	301.6 ± 6.6 Ma	Ma et al., 2020
11	Jalaid Banner (47°24′01″N, 122°17′19″E)	Monzogranite	Zr.LA-ICP-MS	320.6 ± 3.7 Ma	Ma et al., 2020
12	Jalaid Banner (47°24′02″N, 122°18′42″E)	Biotite granodiorite	Zr.LA-ICP-MS	305.9 ± 1.8 Ma	Ma et al., 2020
13	Jiwen	Metagabbro	SIMS	306.0 ± 8.7 Ma	Feng et al., 2015
14	Jiwen	Metagabbro	SIMS	307.8 ± 7.1 Ma	Feng et al., 2015
15	Langfeng (48°03′30″N, 121°12′27″E)	Syenogranite	Zr.LA-ICP-MS	337.0 ± 8.0 Ma	Wu et al., 2002
16	Lapou (49°29′35″N, 121°13′07″E)	Syenogranite	Zr.LA-ICP-MS	325.0 ± 3.0 Ma	Zhang et al., 2013
17	Longzhen	Biotite monzogranite	Zr.LA-ICP-MS	316 ± 4 Ma	Zhang et al., 2010
18	Moguqi(47°30′22.4″N,122°21′58.7″E)	Rhyolite	Zr.LA-ICP-MS	312.6 ± 2.9 Ma	Ma et al., 2019
19	Moguqi(47°31′15.8″N, 122°20′14.7″E)	Granite popphyry	Zr.LA-ICP-MS	309.8 ± 3.6 Ma	Ma et al., 2019
20	Moguqi(47°32′47.9″N, 122°36′33.8″E)	Monzogranite	Zr.LA-ICP-MS	320.9 ± 3.5 Ma	Ma et al., 2019
21	Moguqi(47°38′42.5″N,122°26′24.7″E)	Rhyolite	Zr.LA-ICP-MS	307.5 ± 2.3 Ma	Ma et al., 2019
22	Molidawa	Monzonitic granite	Zr.LA-ICP-MS	301 ± 2 Ma	Wu et al., 2011
23	Quansheng(47°53′30″N,120°01′59″E)	Syenogranite	Zr.LA-ICP-MS	294.8 ± 1.6 Ma	Cui et al., 2013
24	Quansheng(47°53′30″N,120°01′60″E)	Monzonitic granite	Zr.LA-ICP-MS	301.3 ± 2.6 Ma	Cui et al., 2013
25	Quansheng(47°53′30″N,120°01′61″E)	Monzonitic granite	Zr.LA-ICP-MS	305.9 ± 2.4 Ma	Cui et al., 2013
26	Quansheng(47°53′30″N,120°01′62″E)	Syenogranite	Zr.LA-ICP-MS	322.2 ± 1.2 Ma	Cui et al., 2013
27	Shierzhan (51°11′52″N, 125°40′47″E)	Syenogranite	Zr.LA-ICP-MS	298.0 ± 2.0 Ma	Sui et al., 2009
28	Taerqi	Granodiorite	Zr.LA-ICP-MS	320 ± 1 Ma	Wu et al., 2011
29	Taerqi (47°58′35″N, 121°11′15″E)	Syenogranite	Zr.LA-ICP-MS	335.0 ± 5.0 Ma	Zhang et al., 2011
30	Taerqi (47°58′35″N, 121°11′16″E)	Monzonitic granite	Zr.LA-ICP-MS	313.0 ± 3.0 Ma	Zhang et al., 2011
31	Taerqi (47°58′35″N, 121°11′17″E)	Granodiorite	Zr.LA-ICP-MS	320.0 ± 1.0 Ma	Zhang et al., 2011
32	Tahe(52°26′33″N,124°50′06″E)	Gabbro	Zr.LA-ICP_MS	333.0 ± 8.0 Ma	Zhou et al., 2005
33	Tayuan	Metagabbro	SIMS	311.8 ± 2.8 Ma	Feng et al., 2015
34	Tayuan	Metagabbro	SIMS	314.9 ± 2.5 Ma	Feng et al., 2015
35	Tayuan	Granite	Zr.LA-ICP-MS	329.4 ± 2.4 Ma	Feng et al., 2015
36	Tayuan	Metagarrbo	Zr.LA-ICP-MS	331.0 ± 2.6 Ma	Feng et al., 2015
37	Tayuan (51°29′49″N, 124°23′05″E)	Monzonitic granite	Zr.LA-ICP-MS	318.0 ± 4.0 Ma	Wu et al., 2011
38	Tayuan (51°29′49″N, 124°23′05″E)	Gabbro	Zr.LA-ICP-MS	322.0 ± 5.0 Ma	Wu et al., 2011
39	Xing'an (48°48′26″N, 121°42′11″E)	Monzonitic granite	Zr.LA-ICP-MS	309.0 ± 4.0 Ma	Wu et al., 2002
40	Xing'an	Monzonitic granite	Zr.LA-ICP-MS	309 ± 4 Ma	Wu et al., 2011
41	Xing'an	Monzonitic granite	Zr.LA-ICP-MS	309 ± 4 Ma	Wu et al., 2011
42	Yakeshi (49°34′38″N, 121°16′27″E)	Granodiorite	Zr.SHRIMP	331.2 ± 3.7 Ma	Zhao et al., 2010
43	Zhalantun (48°00′12″N, 122°46′19″E)	Syenogranite	Zr.LA-ICP-MS	301.0 ± 3.0 Ma	Wu et al., 2002
44	Zhengdashan	Monzonitic granite	Zr.LA-ICP-MS	315 ± 4 Ma	Zhang et al., 2010

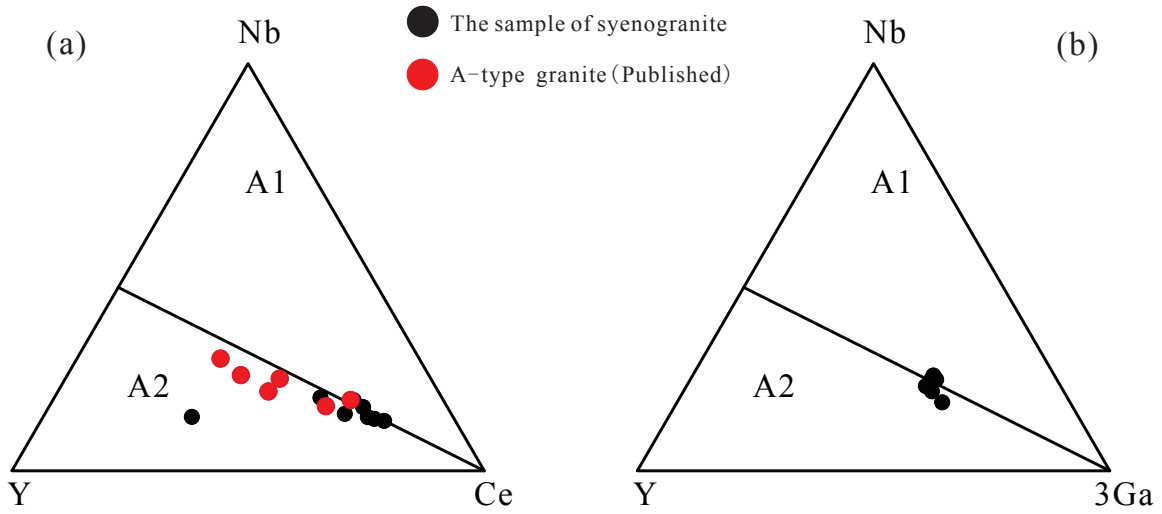

Figure 12. (a) Y–Nb–Ce diagram. (b) Y–Nb–3Ga diagram (modifiedafter Eby et al., 1992) for the Late Carboniferous Chaihe granitoids (published data from Mao et al., 2019). A1: A1-type granites; A2: A2-type granites.

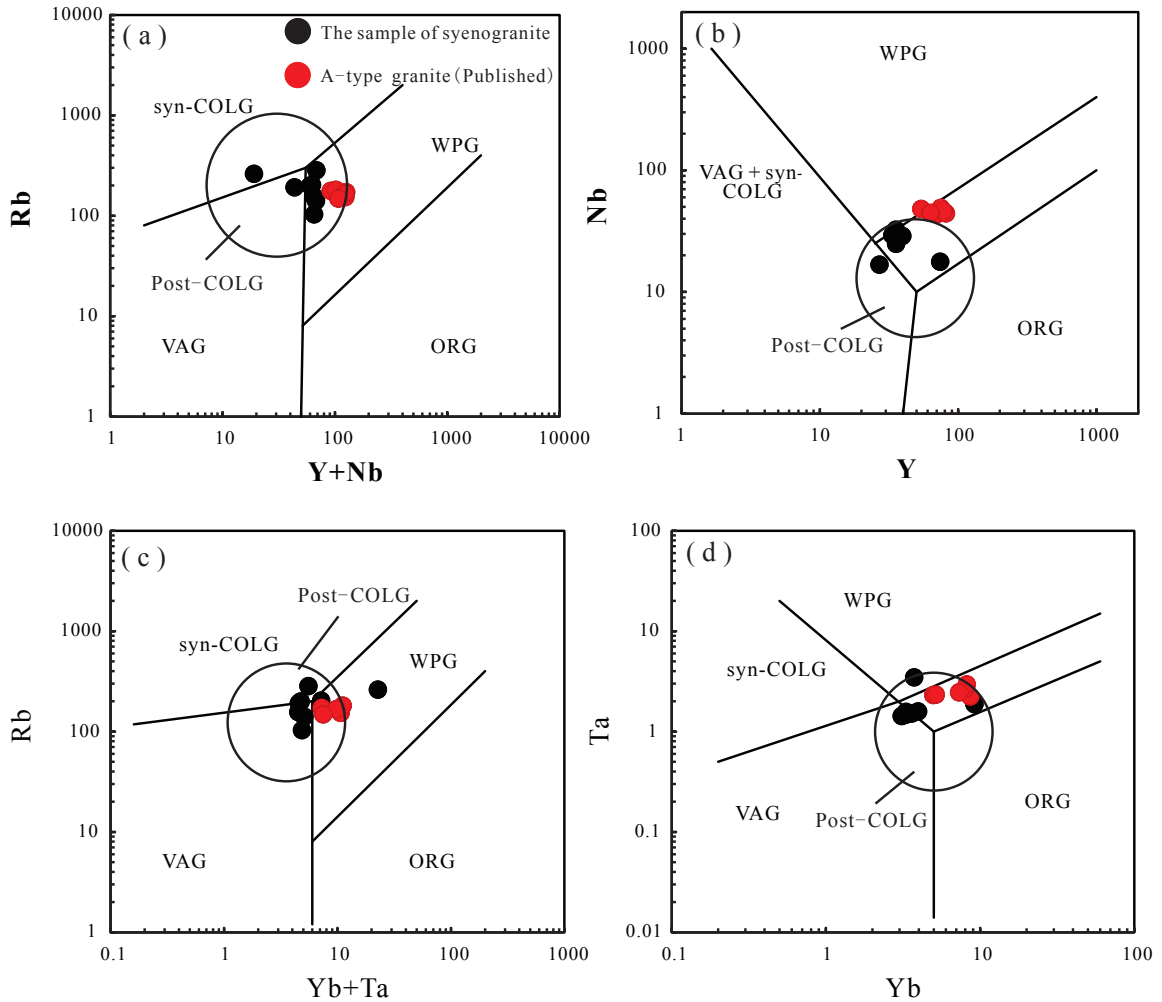

Figure 13. Tectonic discrimination diagrams (modified after Pearce et al., 1984; reported data from Mao et al., 2019). VAG: volcanic arc granite; Syn-COLG: syn-collision granite; WPG: within-plate granite; ORG: ocean-ridge granite; FG: fractionated felsic granites; OTG: unfractionated M-, I-, and S-type granites.

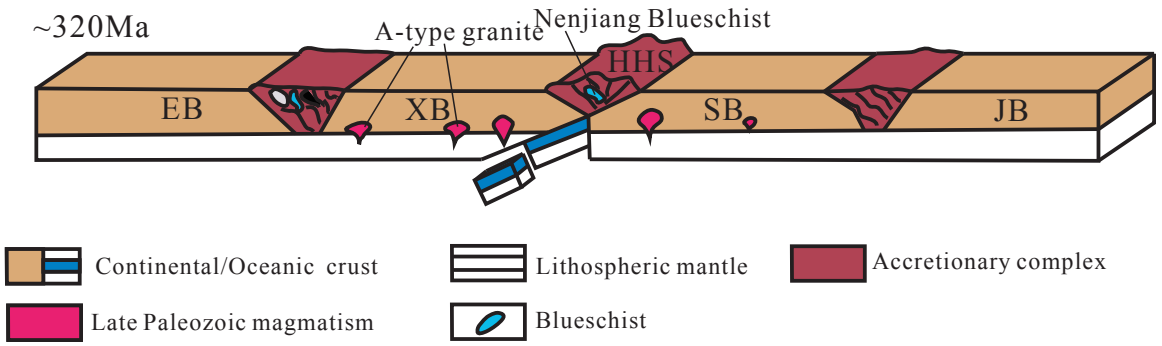

Figure 14. Carton model for the tectonic evolution of the micro-blocks in NE China during Late Carboniferous (modified after Liu et al.,2017. EB: Erguna Block; XB: Xing'an Block; SB: Songnen Block; JB: Jiamusi Block; HHS: Hegenshan-Heihe suture; MYS: Mudanjiang-Yilan suture).

two blocks should have occurred in the Early Mesozoic. The late Paleozoic magma activity was related to the local strike-slip pull-off of the oceanic crust subducted slabs before the collision, but it is difficult to explain the large-area outcrops of newly discovered post-orogenic granites in recent years. These granite bodies may not only be caused by the separation of subducting slabs, but their formation should be related to the extension and thinning of the crust after the Xing'an and Songnen blocks were combined. Studies have shown that, after the closure of the Paleo-Asian Ocean, the Hegenshan Backarc Basin subduction movement still exists in the region. The same small-scale orogenic movement can exist in the post-orogenic stage (Zhang et al., 2011), and there is a tectonic cycle from subduction to collision in the Carboniferous-Permian (Jian et al., 2010), Hegenshan area The gabbro (290~298Ma) related to subduction may be the product of this tectonic cycle.

Based on the above and previous studies, we believe that the Xing'an block and the Songnen block had collided and merged before the Late Carboniferous (~320 Ma), and the Late Carboniferous was in the post-orogenic extension stage (Figure 14).

7. Conclusion

The syenogranites are rich in LREEs and LILEs, and are depleted in HREEs and HFSEs, which characterize them as the typical A-type granites. It was formed by partial melting of the crust under a post-collisional extensional tectonic setting.

LA-ICP-MS U-Pb analysis of zircons from the syenogranites in the Chaihe area indicates that magmatism event developed in the late Carboniferous around 303.1–316.1 Ma.

The Late Carboniferous syenogranites in the HHS A-type granite belt in the eastern segment of the CAOB formed in a post-collisional extensional tectonic setting that was controlled by processes of delamination and asthenospheric upwelling that took place after the closure of the Nenjiang Ocean caused by the amalgamation of the Xing'an and Songnen blocks.

Acknowledgment

This project was financially co-supported by the National Natural Science Foundation of China (Grant No. 41872192) and the 250,000 Chaihe and Moguqi Area Adjustment and Testing Project (Grant No. 1212011120654). We thank Dr. Yujie Hao from the Key Laboratory of Mineral Resources Evaluation in Northeast Asia, Ministry of Natural Resources, for his kindly help with the analysis of the zircon LA-ICP-MS U-Pb ages. Thanks also due to Gou Jun from the School of Earth Science Education, Jilin University, for review, which significantly improved the manuscript. We acknowledge the detailed comments of three anonymous journal reviewers and editor Prof. Baochun Huang who helped clarify ideas and presentation.

References

Bai WJ, Li H, LeBel L (1985). A discussion of the chromite deposits genetic conditions contained in the Hegenshan ophiolite complex at Inner Mongolia China Proceedings of the Chinese. Academy of Geological Sciences 12: 1-19. (in Chinese)

Bao QZ, Zhang CJ, Wu ZL (2011). New geological evidences for the forming age of Wusinihei ophiolitic mélange in Inner Mongolia. Geology and Resources 20: 16-20. (in Chinese with English abstract).

Barbarin B (1999). A review of the relationships between granitoid types origins and their geodynamic environments. Lithos 46: 605-626 doi: 10.1016/S0024-4937(98)00085-1

Boynton WV (1984). Geochemistry of the rare earth elements: meteorite studies. Rare Earth Element Geochemistry 23-114 doi: 10.1016/B978-0-444-42148-7.50008-3

Chen B, Jahn BM, Wilde S, Xu B (2000). Two contrasting Paleozoic magmatic belts in northern Inner Mongolia China: petrogenesis and tectonic implications. Tectonophysics 328 (1-2): 157-182. doi: 10.1016/S0040-1951(00)00182-7

Collins WJ, Beams SD, White AJR, Chappell BW (1982). Nature and origin of A-type granites with particular reference to southeastern Australia. Contributions to Mineralogy and Petrology 80: 189-200. doi: 10.1007/BF00374895

Cui FH, Zheng CQ, Xu XC, Yao WG, Shi L et al. (2013). Late Carboniferous magmatic activity in Quansheng Forest Farm area of Daxing'anling: Limitation of the time when the Xing'an block and Songnen block were combined(J). Acta Geology 87 (09): 1247-1263 (in Chinese with English abstract).

Eby GN (1992). Chemical subdivision of the a-type granitoids: petrogenetic and tectonic implications. Geology 20 (7): 641. doi: 10.1130/0091-7613(1992)020<0641: CSOTAT>2.3.CO;2

Eby GN (1990). The A-type granitoids: a review of their occurrence and chemical characteristics and speculations on their petrogenesis. Lithos 26 (1-2): 115-134. doi: 10.1016/0024-4937(90)90043-Z

Feng ZQ, Jia J, Liu YJ, Wen QB, Li WM et al. (2015). Geochronology and geochemistry of the Carboniferous magmatism in the northern Great Xing'an Range NE China: Constraints on the timing of amalgamation of Xing'an and Songnen blocks. Journal of Asian Earth Sciences 113: 411-426. doi: 10.1016/j.jseaes.2014.12.017

Feng ZQ, Li WM, Liu YJ, Jin W, Wen QB et al. (2018). Early Carboniferous tectonic evolution of the northern Heihe-Nenjiang-Hegenshan suture zone NE China: constraints from the mylonitized Nenjiang rhyolites and the Moguqi gabbros. Geological Journal 53 (3): 1005-1021. doi: 10.1002/gj.2940

Feng ZQ, Liu YJ, Jin W, Li WM, Wen QB (2017). Is there the Paleoproterozoic komatiite related to mantle plume in the Jifeng area Northern Great Xing'an Range NE China? Reply to the comments on: "Timing and nature of the Xinlin-Xiguitu Ocean: Constraints from ophiolitic gabbros in the northern Great Xing'an Range eastern Central Asian Orogenic Belt" by Ni. International Journal of Earth Sciences 106: 2225-2231. doi: 10.1007/s00531-016-1413-1

Feng ZQ, Liu YJ, Liu BQ, Wen QB, Li WM (2016). Timing and nature of the Xinlin-Xiguitu Ocean: constraints from ophiolitic gabbros in the northern Great Xing'an Range, eastern Central Asian Orogenic Belt. International Journal of Earth Sciences 105 (2): 491-505. doi: 10.1007/s00531-015-1185-z

Frost BR, Barnes CG, Collins WJ, Arculus RJ, Ellis DJ et al. (2001). A geochemical classifcation for granitic rocks. Journal of Petrology 42 (11): 2033-2048. doi: 10.1093/petrology/42.11.2033

Ge WC, Sui ZM, Wu FY, Zhang JH, Xu XC et al. (2007). Zircon U-Pb ages, Hf isotopic characteristics and their implications of the Early Paleozoic granites in the northern Da Hinggan Mts northeastern China. Acta Petrologica Sinica 23 (2): 423-440 (in Chinese with English abstract).

Ge WC, Wu FY, Zhou CY, Abdel RA (2005). A Emplacement age of the Tahe granite and its constraints on the tectonic nature of the Erguna block in the northern part of the Da Xing'an Range. Chinese Science Bulletin 50 (18): 2097-2105 (in Chinese with English abstract).

Guo FF, Jiang CY, Su CK, Xia MZ, Xia ZD et al. (2008). Tectonic settings of A-type granites of Shaerdelan area southeastern margin of Junggar block Xinjiang western China. Acta Petrologica Sinica 24 (12): 2778-2788 (in Chinese with English abstract).

Han GQ, Liu YJ, Neubauer F, Bartel E, Genser J et al. (2015). U-Pb age and Hf isotopic data of detrital zircons from the Devonian and Carboniferous sandstones in Yimin area NE China: New evidences to the collision timing between the Xing'an and Erguna blocks in eastern segment of Central Asian Orogenic Belt. Journal of Asian Earth Sciences 97 (Part B): 211-228. doi: 10.1016/j.jseaes.2014.08.006

Han GQ, Liu YJ, Neubauer F, Genser J, Li W et al. (2011). Origin of terranes in the eastern Central Asian Orogenic Belt NE China: U-Pb ages of detrital zircons from Ordovician-Devonian sandstones North Great Xing'an Range. Tectonophysics 511 (3-4): 109-124. doi: 10.1016/j.tecto.2011.09.002

Han GQ, Liu YJ, Neubauer F, Genser J, Ren SM et al. (2012). LA-ICP-MS U-Pb dating and Hf isotopic compositions of detrital zircons from the Permian sandstones in Da Xing'an Mountains NE China: New evidence for the eastern extension of the Erenhot- Hegenshan suture zone. Journal of Asian Earth Sciences 49: 249-271. doi: 10.1016/j.jseaes.2011.11.011

Hao YJ, Ren YS, Duan MX, Tong KY, Chen C et al. (2015). Metallogenic events and tectonic setting of the Duobaoshan ore field in Heilongjiang Province NE China. Journal of Asian Earth Sciences 97 (Part B): 442-458. doi: 10.1016/j.jseaes.2014.08.007

HBGMR (Heilongjiang Bureau of Geology and Mineral Resources) (1993). Regional geology of Heilongjiang Province. Geological Publishing House. pp: 57-734. (in Chinese with English abstract)

Hong DW, Huang HZ, Xiao YJ, Xu HM, Jin MY (1994). The Permian alkalinegranites in center Innher Mongolia and their geodynamic significance. Acta Geologica Sinica 68 (3): 219-230 (in Chinese with English abstract).

Hong DW,Huang HZ, Xiao YJ, Xu HM, Jin MY (1995). Permian alkaline granites in central Inner Mongolia and their geodynamic significance. Acta Geologica Sinica (1) 8: 27-39. doi: 10.1111/j.1755-6724.1995.mp8001003.x

Hoskin PO, Schaltegger U (2003). The composition of zircon and igneous and metamorphic petrogenesis. Reviews in Mineralogy and Geochemistry 53(1): 27-62.

Hu DG, Tan CX, Zhang H (1995). Middle Proterozoic ophiolites in the Alihe area Inner Mongolia. Region Geology China 4: 334-339 (in Chinese with English abstract).

Irvine TN, Baragar WRA (1971). A guide to the chemical classification of the common volcanic rocks. Canadian Journal of Earth Sciences 8 (5): 523-548. doi: 10.1139/e71-055

Jahn BM, Windley B, Natal'in B, Dobretsov N (2004). Phanerozoic continental growth in Central Asia. Journal of Asian Earth Sciences 23 (5): 599-603. doi: 10.1016/S1367-9120(03)00124-X

Jian P, Liu DY, Kröner A, Windley BF, Shi YR et al. (2010). Evolution of a Permian intra oceanic arc-trench system in the Solonker suture zone Central Asian Orogenic Belt China and Mongolia. Lithos 118 (1): 169-190. doi: 10.1016/j.lithos.2010.04.014

Jiang SY, Zhao KD, Jiang YH, Dai BZ (2008). Characteristics and genesis of Mesozoic a-type granites and associated mineral deposits in the southern Hunan and northern Guangxi provinces along the Shi-Hang Belt South China. Geological Journal of China Universities 14 (4): 496-509 (in Chinese with English abstract).

Li CL, Qu H, Zhao ZH, Xu GZ, Wang Z et al. (2013). Zircon U-Pb ages geochemical characteristics and tectonic implications of Early Carboniferous granites in Huolongmen area Heilongjiang Province. Geology in China 40: 859-868. (in Chinese with English abstract).

Li JY (2006). Permian geodynamic setting of Northeast China and adjacent regions: Closure of the Paleo-Asian Ocean and subduction of the Paleo-Pacific plate. Journal of Earth Science 26 (3-4): 207-224. doi: 10.1016/j.jseaes.2005.09.001

Li RS (1991). Xinlin Ophiolite. Heilongjiang Geology 2: 19-32 (in Chinese with English abstract).

Li S, Wilde S, Wang T, Guo QQ (2016). Latest Early Permian granitic magmatism in southern Inner Mongolia China: Implications for the tectonic evolution of the southeastern Central Asian Orogenic Belt. Gondwana Research 29 (1): 168-180.

Li XW, Mo XX, Zhao ZD, Zhu DC (2010). A discussion on how to discriminate a-type granite. Geological Bulletin of China 29 (2): 278-285 (in Chinese with English abstract).

Li Y, Xu WL, Wang F, Tang J, Pei FP et al. (2014). Geochronology and geochemistry of late Paleozoic volcanic rocks on the westernmargin of the Songnen-Zhangguangcai Range Massif NE China: Implications for the amalgamation history of the Xing'an and Songnen-Zhangguangcai Range massifs. Lithos 205: 394-410.

Liu G, Lv XB, Zhang L, Cao XF, Chen Y et al. (2012). Geochemical characteristics of Early Carboniferous volcanic rock in Hongyan area of northwestern Xiao Hinggan Mountains and their geological significance. Acta Petologica et Mineralogica 31 (5): 641-651 (in Chinese with English abstract).

Liu YJ, Li WM, Feng ZQ, Wen QB, Franz N et al. (2017). A review of the Paleozoic tectonics in the eastern part of Central Asian Orogenic Belt. Gondwana Research 43: 123-148. doi: 10.1016/j.gr.2016.03.013

Liu YJ, Zhang XZ, Chi XG, Wen QB, Liang CY et al. (2011). Deformation and tectonic layer division of the Upper Paleozoic in Daxing'anling area. Journal of Jilin University (Earth Science Edition) 41: 1304-1310 (in Chinese with English abstract).

Liu YJ, Zhang XZ, Jin W, Chi XG, Wang CW et al. (2010). Late Paleozoic tectonic evolution in Northeast China. Geology in China 37: 943-951 (in Chinese with English abstract).

Liu YS, Hu ZC, Gao S, Gunther D, Xu J et al. (2008). In situ analysis of major and trace elements of anhydrous minerals by LA-ICP-MS without applying an internal standard. Chemical Geology 257: 3443. doi: 10.1016/j.chemgeo.2008.08.004

Ludwing KR (2003). ISOPLOT 3.75: a geochronological toolkit for Microsoft Excel Geochronology Centre Special Publication 4: 1-75.

Ma YF, Liu YJ, Wang Y, Qin T, Chen HJ et al. (2020). Late Carboniferous mafic to felsic intrusive rocks in the central Great Xing'an Range NE China: petrogenesis and tectonic implications. International Journal of Earth Sciences 109 (3): 761-783. doi: 10.1007/s00531-020-01828-6

Ma YF, Liu YJ, Wang Y, Tang Z, Qian C et al. (2019). Geochronology and geochemistry of the Carboniferous felsic rocks in the central Great Xing'an Range NE China: implications for the amalgamation history of Xing'an and Songliao-Xilinhot blocks. Geological Journal 54: 482-513. doi: 10.1002/gj.3198

Mao C, Lv XB, Chen C (2019). Geochemical Characteristics of A-Type Granite near the Hongyan Cu-Polymetallic Deposit in the Eastern Hegenshan-Heihe Suture Zone NE China: Implications for Petrogenesis Mineralization and Tectonic Setting. Minerals 9 (5) 309. doi: 10.3390/min9050309.

Miao LC, Fan WM, Liu DY, Zhang FQ Shi YR et al. (2008). Geochronology and geochemistry of the Hegenshan Ophiolitic Complex: Implications for late-stage tectonic evolution of the Inner Mongolia-Daxinganling Orogenic Belt China. Journal of Asian Earth Sciences 32: 348-370. doi: 10.1016/j.jseaes.2007.11.005

Miao LC, Fan WM, Zhang FQ, Liu DY, Jian P et al. (2004). Zircon SHRIMP geochronology of the Xinkailing-Kele complex in the northwestern Lesser Xing'an Range and its geological implications. Chinese Science Bulletin 49: 201-209. doi: 10.1016/j.envsci.2013.05.002

Miao LC (2003). SHRIMP zircon geochronological studies of the Da Hinggan Mountains. Report of the postdoctoral research. Beijing, China: Chinese Academy of Sciences Institute of Geology and Geophysics

Middlemost EAK (1994). Naming materials in the magma/igneous rock system. Earth-Science Reviews 37: 215-224. doi: 10.1016/0012-8252(94)90029-9

Nozaka T, Liu Y (2002). Petrology of the Hegenshan ophiolite and its implication for the tectonic evolution of northern China. Earth and Planetary Science Letters 202 (1): 89-104. doi: 10.1016/S0012-821X(02)00774-4

Pearce JA, Harris NBW, Tindle AG (1984). Trace element discrimination diagrams for the tectonic interpretation of granitic rocks. Journal of Petrology 25 (4): 956-983. doi: 10.1093/petrology/25.4.956

Pearce JA (1983). Role of the sub-continental lithosphere in magma genesis at active continental margins. Journal of the Electrochemical Society 147 (6). doi: 10.1149/1.1393502

Peccerillo A, Taylor SR (1976). Geochemistry of Eocene calc-alkaline volcanic rocks from the Kastamonu Area, Northern Turkey. Contributions to Mineralogy and Petrology 58 (1): 63-81. doi: 10.1007/BF00384745

Qian C, Lu L, Qin T, Li LC, Chen HJ et al. (2018). The early late Paleozoic granite in the Zhalantun area of the northern part of the Great Xing'an Mountains magmatism: constraints on the time limit of the integration of the Ergun-Xing'an and Songnen blocks. Acta Geologica Sinica 92 (11): 2190-2214.

Qu H, Li CL, Zhao ZH, Wang Z, Zhang JF (2011). Zircon U-Pb ages and geochemical characteristics of the granites in Duobaoshan area Northeast Da Hinggan Mountains. Geology China 38: 292-300 (in Chinese with English abstract).

Şengör AMC, Natal'in B (1996). Paleotectonics of Asia: fragments of a synthesis In: Yin A Harrison M (editors). The Tectonic Evolution of Asia. Cambridge, UK: Cambridge University Press, pp. 486-640.

Şengör AMC, Natal'in BA, Burtman US (1993). Evolution of the Altaid tectonic collage and Paleozoic crustal growth in Eurasia. Nature 364: 209-304.

Şengör AMC, Natal'In BA, Gürsel S, vander Voo R (2018). The tectonics of the Altaids: crustal growth during the construction of the continental lithosphere of Central Asia between ~750 and ~130 Ma Ago. Annual Review of Earth Planetsry Sciences 46 (1): 439-494. doi: 10.1146/annurev-earth-060313-

Shao JA (1991). Crustal evolution in the middle part of the Northern Margin of the Sino-Korean Plate. In: Zhang LM (editor). Peking, China: Peking University, pp. 1-136. (in Chinese)

Shi GH, Miao LC, Zhang FQ, Jian P, Fan WM et al. (2004). The age and its district tectonic implications on Xilinhot A-type granites Inner Mongolia. Chinese Science Bulletin 49 (4): 384-389 (in Chinese with English abstract)

Shi Y, Yao Y, Liu ZH, Liu J, Wei MH et al. (2019). Petrogeochemical characteristics zircon SHRIMP U-Pb ages and Lu-Hf isotopic compositions of Late Carboniferous A-type granitoids Yili area Inner Mongolia (China). Geological Journal 54 (2): 770-790. doi: 10.1002/gj.3406

Su YZ (1996). Paleozoic stratigraphy of Xing'an stratigraphical province Jilin. Geology 15 (3-4): 23-34. (in Chinese with English abstract)

Sui ZM, Ge WC, Wu FY, Xu XC, Wang HQ (2006). U-Pb chronology in zircon from Harabaqi granitic pluton in northeastern Greater Xing'an Mountains area and its origin Global. Geology 25 (3): 229-236. (in Chinese with English abstract)

Sui ZM, Ge WC, Wu FY, Xu XC, Zhang JH (2009a). Hf isotopic characteristics and geological significance of the Chahayan pluton in Northern Da xing'an Ling Mountains Journal of Jilin University (Earth Science Edition) 39 (5): 849-856. (in Chinese with English abstract)

Sui ZM, Ge WC, Xu XC, Zhang JH (2009b). Characters and geological implications of the late Paleozic post-orogenic Shierzhan granite in the Great Xing'an Range. Acta Petrologica Sinica 25: 2679-2686. (in Chinese with English abstract)

Sun DY, Wu FY, Li HM, Lin Q. (2000). Emplacement age of the post-orogenic A-type granites in Northwestern Lesser Xing'an Range and its relationship to the eastward extension of Suolushan-Hegenshan-Zhalaite collisional suture zone. Chinese Science Bulletin 45(20): 2217-2222 (in Chinese with English abstract)

Sun DY, Wu FY, Li HM, Lin Q (2001). Emplacement age of the postorogenic Atype granites in Northwestern Lesser Xing'an Ranges and its relationship to the eastward extension of Suolunshan-Hegenshan-Zhalaite collisional suture zone. Chinese Science Bulletin 46 (5): 427-432. (in Chinese with English abstract)

Sun SS, McDonough WF (1989). Chemical and isotopic systematics of oceanic basalts: implications for mantle composition and processes. Geological Society London 42 (1): 313-345. doi: 10.1144/GSL.SP.1989.042.01.19

Tang KD (1990). Tectonic development of Paleozoic fold belts at the northern margin of the Sino-Korean Craton. Tectonics 9 (2): 249-260. doi: 10.1029/TC009i002p00249

Tian DX, Yang H, Ge WC, Zhang YL, Chen JS et al. (2018). Petrogenesis and tectonic implications of Late Carboniferous continental arc high-K granites in the Dongwuqi area central Inner Mongolia North China(J). Journal of Asian Earth Sciences 167: 82-102. doi:10.1016/j.jseaes.2018.07.010

Tong Y, Hong DW, Wang T, Shi XJ, Zhang JJ et al. (2010). Spatial and temporal distribution of granitoids in the middle segment of the Sino-Mongolian Border and its tectonic and metallogenic implications. Acta Geoscientica Sinica 31 (3): 395-412. (in Chinese with English abstract)

Wang Y, Fu JY, Na FC, Liu YC, Zhang GY et al. (2013). Geochemical characteristics and zircon U-Pb age of the gabbro-diorite in Jalaid Banner of Inner Mongolia and their geological significance. Geol Bullet China 32: 1525- 1535.

Wang YQ (1996). Pre-Cambrian stratigraphy of northeastern China Jilin Geology 15 (3-4): 1-14. (in Chinese with English abstract)

Whalen JB, Currie KL, Chappell BW (1987). A-type granites: Geochemical characteristics discrimination and petrogenesis. Contributions to Mineralogy and Petrology 95 (4): 407-419.

Wilde SA, Wu FY, Zhang XZ (2003). Late Pan-African magmatism in Northeastern China: SHRIMP U-Pb zircon evidence for igneous ages from the Mashan Complex. Precambrian Research 122: 311-327.

Wilde SA, Zhang XZ, Wu FY (2000). Extension of a newly-identified 500 Ma metamorphic terrain in Northeast China: Further U-Pb SHRIMP dating of the Mashan Complex Heilongjiang Province China. Tectonophysics 328 (1): 115-130. doi: 10.1016/S0040-1951(00)00180-3

Wu FY, Jahn BM, Wilde SA, Lo CH, Yui TF et al. (2003). Highly fractionated I-type granites in NE China (I): Geochronology and petrogenesis. Lithos 66 (3-4): 241-273. doi: 10.1016/S0024-4937(02)00222-0

Wu FY, Jahn BM, Wilde SA, Sun DY (2000). Phanerozoic continental crustal growth: U-Pb and Sr-Nd isotopic evidence from the granites in northeastern China. Tectonophysics 328 (1): 87-113. doi: 10.1016/S0040-1951(00)00179-7

Wu FY, Sun DY, Ge WC, Zhang YB, Grant ML et al. (2011). Geochronology of the Phanerozoic granitoids in northeastern China. Journal of Asian Earth Sciences 41 (1): 1-30. doi: 10.1016/j.jseaes.2010.11.014

Wu FY, Sun DY, Li HM, Jahn BM, Wilde SA (2002). A-type granites in northeastern China: Age and geochemical constraints on their petrogenesis. Chemical Geology 187 (1-2): 143-173. doi: 10.1016/S0009-2541(02)00018-9

Wu FY, Sun DY, Li HM, Wang XL (2001). The nature of basement beneath the Songliao Basin in NE China: Geochemical and isotopic constraints. Physics and Chemistry of the Earth (Part A) 26 (9): 793-803. doi: 10.1016/S1464-1895(01)00128-4

Wu G, Sun FY, Zhao SC, Li ZT, Zhao AL et al. (2005). Discovery of the Early Paleozoic post-collisional granites in the Northern margin of the Erguna massif and its geological significance. Chinese Science Bulletin 50 (23): 2733-2743 doi: 10.1360/982004-679. (in Chinese with English abstract)

Xiao WJ, Windley BF, Hao J, Zhai MG (2003). Accretion leading to collision and the Permian Solonker suture Inner Mongolia China: Termination of the Central Asian Orogenic Belt. Tectonics 22: 1069- 1090. doi: 10.10029/2002TC001484

Xiao WJ, Windley BF, Sun S, Li JL, Huang BC et al. (2015). A tale of amalgamation of three permotriassic collage systems in Central Asia: oroclines sutures and terminal accretion. Annual Review of Earth and Planetary Sciences 43: 477-507. doi: 10.1146/annurev earth-060614-105254.

Xu B, Charvet J, Chen Y, Zhao P, Shi G (2013). Middle Paleozoic convergent orogenic belts in western Inner Mongolia (China): Framework kinematics geochronology and implications for tectonic evolution of the Central Asian Orogenic Belt. Gondwana Research 23 (4): 134-264. doi: 10.1016/j.gr.2012.05.015

Xu B, Chen B (1997). Framework and evolution of the middle Paleozoic orogenic belt between Siberian and North China Plates in northern Inner Mongolia. Science China (Ser D) 40 (5): 463-469. doi: 10.1007/BF02877610

Xu B, Zhao P, Bao QZ, Wang YY, Luo ZW (2014). Preliminary study on the pre-Mesozoic tectonic unit division of the Xing-Meng orogenic belt (XMOB). Acta Petrologica Sinica 30 (7): 1841-1857. doi: 10.1016/j.pgeola.2014.02.004 (in Chinese with English abstract)

Zhang J, Chen JS, Li BY, Gao Y, Zhang YL (2011). Zircon U-Pb ages and Hf isotopes of Late Paleozoic granites in Taerqi area Inner Mongolia. Global Geology 30 (4): 521-531. doi: 10.1021/ed1002509 (in Chinese with English abstract)

Zhang L, Liu YJ, Li WM, Han GQ, Zhang JD et al. (2013a). Discussion on the basement properties and east boundary of the Erguna Massif. Chinese Journal of Geology 48 (1): 227-244. doi: 10.3969/j.issn.0563-5020.2013.01.015 (in Chinese with English abstract)

Zhang L, Lv XB, Liu G, Chen J, Chen C et al. (2013b). Characteristics and genesis of continental back-arc A-type granites in the eastern segment of the Inner Mongolia-Da Hinggan Mountains orogenic belt. Geology in China 40 (3): 869-884.

Zhang Q, Wang Y, Li CD, Wang YL, Jin WJ et al. (2006). Sr-Yb classification of granite and its geological significance(J). Acta Petrologica Sinica 09: 2249-2269.

Zhang Q, Wang Y, Pan GQ, Li CD, Jin WJ (2008). The source rock problem of granite——The fourth thought on granite research(J). Acta Petrologica Sinica 24 (06): 1193-1204.

Zhang XZ, Zhou JB, Chi XG, Wang CW, Hu DQ (2008). Late Paleozoic Tectonic Sedimentation and Petroleum Resources in Northeastern China. Journal of Jilin University (Earth Science Edition) 38 (5): 719-725. doi: 10.1002/clen.200700058

Zhang YL, Ge WC, Gao Y, Chen JS, Zhao L (2010). Zircon U-Pb ages and Hf isotopes of granites in Longzhen area and their geological implications. Acta Petrologica Sinica 26 (4): 1059-1073. doi: 10.1016/S0016-5085(15)31930-2 (in Chinese with English abstract)

Zhang ZC, Li K, Li JF, Tang WB, Chen Y et al. (2015). Geochronology and geochemistry of the eastern Erenhot ophiolitic complex : Implications for the tectonic evolution of the Inner Mongolia_ Daxinganling orogenic belt. Journal of Asian Earth Science 97: 279-293. doi: 10.1016/j.jseaes.2014.06.008

Zhao P, Fang JQ, Xu B, Chen Y, Michel Faure (2014). Early Paleozoic tectonic evolution of the Xing-Mengorogenic belt: Constraints from detrital zircon geochronology of western Erguna-Xing'an Block North China. Journal of Asian Earth Sciences 95 (38): 136-146. doi: 10.1016/j.jseaes.2014.04.011

Zhao Z, Chi XG, Liu JF, Wang TF, Hu ZC (2010a). Late Paleozoic arc-related magmatism in Yakeshi region Inner Mongolia: Chronological and geochemical evidence. Acta Petrologica Sinica 26 (11): 3245-3258. (in Chinese with English abstract)

Zhao Z, Chi XG, Pan SY, Liu JF, Sun W et al. (2010b). Zircon U-Pb LA-ICP-MS dating of Carboniferous volcanics and its geological significance in the northwestern Lesser Xing'an Range. Acta Petrologica Sinica 26 (8): 2452-2464. doi: 10.3724/SP.J.1084.2010.00199 (in Chinese with English abstract)

Zheng YF, Xiao WJ, Zhao GC (2013). Introduction to tectonics of China. Gondwana Research 23 (4): 1189-1206. doi: 10.1016/j.gr.2012.10.001

Zhou CY, Wu FY, Ge WC, Sun DY, Abdel Rahman AA et al. (2005). Age geochemistry and petrogenesis of the cumulate gabbro in Tahe northern Great Xing'an Range. Acta Petrologica Sinica 21 (3): 763-775. doi: 10.1016/j.sedgeo.2005.01.008 (in Chinese with English abstract)

Zhou HS, Ma CQ Zhang C, Chen L, Zhang JY et al. (2008). Yanshanian alnminous A-type granitoids in the Chunshui of Biyang south margin of North China Craton: Implications from petrology geochronology and geochemistry. Acta Petrologica Sinica 24 (1): 49-64. doi: 10.3986/AGS48106 (in Chinese with English abstract)

Zhou JB, Wilde SA (2013). The crustal accretion history and tectonic evolution of the NE China segment of the Central Asian Orogenic Belt. Gondwana Research 23 (4): 1365-1377. doi: 10.1016/j.gr.2012.05.012

Zhou JB, Han J, Zhao GC, Zhang XZ, Cao JL et al. (2015a). The emplacement time of the Hegenshan ophiolite: Constraints from the unconformably overlying Paleozoic strata. Tectonophysics 662: 398-415. doi: 10.1016/j.tecto.2015.03.008

Zhou JB, Wang B, Wildea SA, Zhao GC, Cao JL et al. (2015b). Geochemistry and U-Pb zircon dating of the Toudaoqiao blueschists in the Great Xing'an Range northeast China and tectonic implications. Journal of Asian Earth Sciences 97: 197-210. doi: 10.1016/j.jseaes.2014.07.011

Zhou JB, Wilde SA, Zhang XZ, Liu FL (2012). Detrital zircons from Phanerozoic rocks of the Songliao Block NE China: Evidence and tectonic implications. Journal of Asian Earth Sciences 47: 21-34. doi: 10.1016/j.jseaes.2011.05.004

Zhou JB, Wilde SA, Zhang XZ, Ren SM, Zheng CQ (2011a). Early Paleozoic metamorphic rocks of the Erguna block in the Great Xing'an Range NE China: Evidence for the timing of magmatic and metamorphic events and their tectonic implications. Tectonophysics 499 (1-4): 105-117. doi: 10.1016/j.tecto.2010.12.009

Zhou JB, Wilde SA, Zhang XZ, Zhao GC, Liu FL et al. (2011b). A >1300 km late Pan-African metamorphic belt in NE China: New evidence from the Xing'an block and its tectonic implications. Tectonophysics 509 (3-4): 280-292. doi: 10.1016/j.tecto.2011.06.018

Zhou JB, Wilde SA, Zhao GC, Zhang XZ, Wang H et al. (2010a). Was the easternmost segment of the Central Asian Orogenic Belt derived from Gondwana or Siberia: An intriguing dilemma? Journal of Geodynamics 50 (3-4): 300-317. doi: 10.1016/j.jog.2010.02.004

Zhou JB, Wilde SA, Zhao GC, Zhang XZ, Zheng CQ et al. (2010b). New SHRIMP U-Pb zircon ages from the Heilongjiang Complex in NE China: Constraints on the Mesozoic evolution of NE China. American Journal of Science 310 (9): 1024-1053. doi: 10.2475/09.2010.10

Zhou JB, Wilde SA, Zhao GC, Zhang XZ, Zheng CQ et al. (2010c). Pan-African metamorphic and magmatic rocks of the Khanka Massif NE China: Further evidence regarding their affinity. Geological Magazine 147 (5): 737-749. doi: 10.1017/S0016756810000063